Isogeochemical Characterization of Mountain System Recharge Processes in the Sierra Nevada, California

Sandra Armengol[1]†, Hoori Ajami[1], James O'Sickman[1], Lucia Ortega[2]

[1] Department of Environmental Sciences, University of California, Riverside, CA, USA.

[2] International Atomic Energy Agency (IAEA), Vienna, Austria.

Corresponding author: Sandra Armengol (sarmengo@ucr.edu)

†Department of Environmental Sciences, University of California, Riverside, Room 2319 Geology, Riverside, California 92521.

Key Points:

A multi-tool isogeochemical approach differentiates among mountain recharge pathways.

Incorporating chemical reactions in the End-Member Mixing Analysis strongly improves mixing ratio calculation.

Mountain block recharge originating from the Sierra Nevada accounts on average for more than 50% of recharge in the southern Central Valley.

Keywords: Mountain System Recharge, Hydrogeochemisty, End-Member Mixing Analysis, Mountain Front Recharge, Mountain Block Recharge

`

Abstract

Mountain System Recharge (MRS) processes are the natural recharge pathways in arid and semi-arid mountainous regions. However, MSR processes are often poorly understood and characterized in hydrologic models. Mountains are the primary source of water supply to valley aquifers via multiple pathways including lateral groundwater flow from the mountain block (Mountain-block Recharge, MBR) and focused recharge from mountain streams contributing to mountain front recharge (MFR) at the piedmont zone. Here, we present a multi-tool isogeochemical approach to characterize mountain flow paths and MSR processes in the northern Tulare basin, California. We used groundwater chemistry data to delineate hydrochemical facies and explain the chemical evolution of groundwater from the Sierra Nevada to the Central Valley aquifer. Isotope tracers helped to validate MSR processes. Novel application of End-Member Mixing Analysis (EMMA) using conservative chemical components revealed three MSR end-members: (1) evaporated Ca-HCO_3 water type associated with MFR, (2) non-evaporated Ca-HCO_3 and Na-HCO_3 water types with short residence times associated with shallow MBR, and (3) Na-HCO_3 groundwater type with long residence time associated with deep MBR. We quantified the contribution of each MSR process to the valley aquifer using mixing ratio calculation (MIX). Our results show that deep MBR is a significant component of recharge representing more than 50% of the valley groundwater. Greater hydraulic connectivity between the Sierra Nevada and Central Valley has significant implications for parameterizing Central Valley groundwater flow models and improving groundwater management. Our framework is useful for understanding MSR processes in other snow-dominated mountain watersheds.

1. Introduction

Seasonal snowpacks and glaciers supply water to more than 16% of the global population (Barnett, 2005), and 24% of lowland populations rely on runoff from mountainous watersheds (Viviroli et al., 2020). While the contribution of mountain watersheds to streamflow is well known (Viviroli et al., 2020), the mechanisms of groundwater recharge processes in high-elevation mountain ranges are poorly understood (Gleeson and Manning, 2008). Likewise, the degree of hydraulic connectivity between the mountains and valley-fill aquifers is still uncertain (de Vries and Simmers, 2002). Prolonged droughts and reduced snowpack in the western US have increased reliance on groundwater (Scanlon et al., 2005), causing overexploitation of major aquifers, e.g., California's Central Valley aquifer. Projected increases in the frequency and intensity of droughts, warmer temperatures (Seager et al., 2007; Diffenbaugh et al., 2015), and snow to rain transition (Berghuijs et al., 2014) are expected to alter the magnitude and direction of recharge rates. However, our ability to accurately estimate recharge in mountain catchments is limited due to the complexity of recharge processes and lack of direct recharge observations (Ajami et al., 2011; Bales et al., 2006).

Various terminologies have been used to describe recharge processes in a mountain-valley aquifer system (Markovich et al., 2019). Conceptually, a mountain-valley aquifer system consists of two units: a mountain aquifer unit extending from headwaters to the piedmont zone where mountains intersect alluvial deposits (Welch and Allen, 2012), and a valley bottom aquifer unit with boundaries starting at the piedmont zone. We define five recharge pathways along the mountain-valley aquifer continuum (Figure 1). The two main recharge pathways recharging the mountain aquifer are diffuse and focused Mountain Aquifer Recharge (MAR). Diffuse MAR results from snowmelt and rainfall infiltration into the mountain block and focused MAR is from

streamflow infiltration and seepage from lakes in the mountain block. The three main pathways recharging the valley aquifer are: Diffuse valley aquifer recharge (VAR), due to rainfall and irrigation infiltration in the valley floor; focused mountain front recharge (MFR), because of streamflow infiltration in the piedmont zone; and mountain block recharge (MBR) as a result of lateral subsurface flow from the mountain aquifer unit to the adjacent valley aquifer. MFR and MBR may consist of different flow paths with distinct geochemical signatures and residence time. These pathways are collectively called mountain system recharge (MSR).

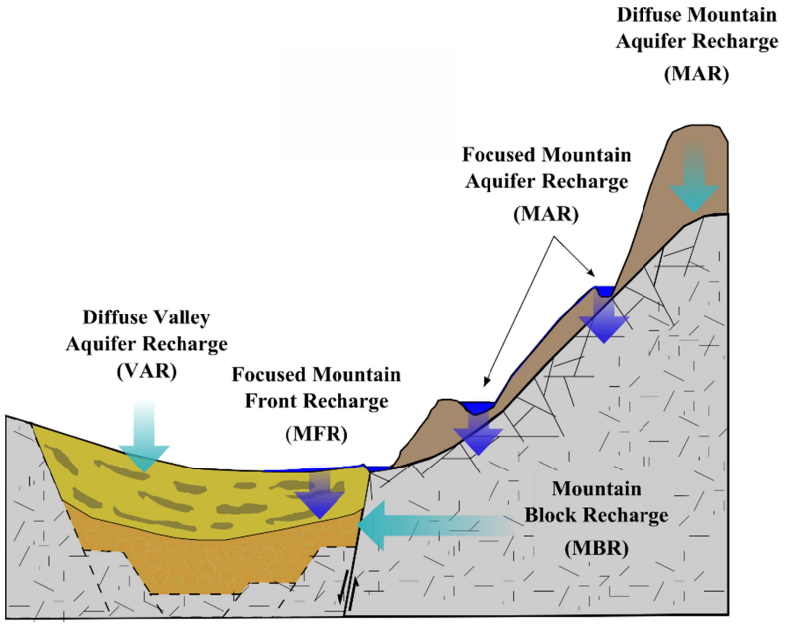

Figure 1. Conceptual illustration of five different recharge pathways in a mountain-valley aquifer system.

MBR and MFR constitute significant recharge components in many arid and semi-arid aquifers (Wilson and Guan, 2004). VAR in arid and semi-arid aquifers is very small due to small precipitation and high evapotranspiration rates. Given differences in infiltration location and residence times of MSR pathways, it is essential to distinguish MSR pathways as they may respond differently to changes in hydroclimate and vegetation conditions (Markovich et al., 2019). While some hydrologists assumed that bedrock is impermeable, the application of geochemical tracers combined with heat and flow modeling demonstrated that MBR contributes 5% to 50% of total recharge (Markovich et al., 2019; Meixner et al., 2016; Aishlin & McNamara, 2011; Manning and Solomon, 2003). A recent synthesis of recharge from mountain aquifers showed that 61 – 93% of MAR discharges via streams (Meixner et al., 2016) and eventually contributes to MFR (Abdulghaffar & Wood, 1996; Coes and Pool, 2007; Goodrich et al., 200; Schreiner-McGraw et al., 2019).

Various methods have been implemented to estimate MSR ranging from empirical relationships (e.g., Maxey-Eakin (1949)) to spatially distributed water balance models such as the Basin Characterization Model (Flint et al., 2004). Accurate MSR quantification requires characterizing the mountain aquifer unit and groundwater circulation depth (Frisbee et al., 2017), as well as the flow paths from the mountain block to the adjacent aquifers. Water balance models require a large amount of data typically unavailable in mountainous catchments due to extreme weather especially during winter, limited access due to complex terrain, and the presence of few

mountain wells. Alternately, the chloride mass balance method (CMB) has been extensively used to estimate recharge rates in mountain catchments (Aishlin & McNamara, 2011). Chloride is considered a conservative solute as it is rarely present in the mountain bedrock and is neither evaporated nor transpired. Bazuhair & Wood (1996) used the CMB method to estimate MBR from the western Saudi Arabia mountains to arid alluvial aquifers. Annual MBR was 3 to 4% of mean annual precipitation with 30 to 50% error in the short-term dataset. In the Dry Creek watershed in Idaho, CMB results showed that 14% of precipitation and 44% of headwater areas contribute to MBR (Aishlin and McNamara, 2011). Annual MBR estimates from the Yucca Mountain in Nevada and Black Mesa in Arizona were 3 to 15 % and 3 to 7% of mean annual precipitation, respectively (Zhu et al., 2003). Application of the CMB method in recharge studies is challenging as chloride retention in soils is not well understood (Shaw et al., 2014), and in low electrical conductivity environments such as snow-dominated mountain systems, chloride is not entirely conservative (Shaw et al., 2014). Furthermore, the CMB method only accounts for a single tracer and more than one tracer is usually needed to describe mixing dynamics in complex mountain-valley systems.

Christopherson and Hooper (1992) and Hooper et al. (1990) combined multiple tracers using a multivariate statistical analysis method, (EMMA), to identify water sources in streamflow. The application of EMMA has been instrumental in identifying MSR sources (e.g., Wahi et al., 2008) and its partitioning. Wahi and others (2008) applied a mixing model using oxygen and hydrogen isotopes in the Upper San Pedro River Basin, Arizona, attributing 70% of the MSR, to winter and 30% to summer precipitation. Peng et al. (2018) applied EMMA to oxygen and hydrogen groundwater isotopes and electrical conductivity (EC) data from three alluvial fans in eastern Taiwan. They attributed 70 % of the MSR to MFR and MBR, and the remainder to VAR. They showed MBR is mainly controlled by the degree of mountain bedrock fracturing, while MFR is impacted by streambed permeability and slope. Liu and Yamanaka (2012) applied EMMA to oxygen and hydrogen groundwater isotopes and major dissolved solutes, and identified distance from the river and topography as important factors controlling MFR. Frisbee et al. (2011) applied EMMA to EC, calcium, magnesium, potassium, silica, and $\delta^{18}O$ and $\delta^{2}H$ of groundwater in two mountain watersheds in the Southwestern United States. They determined a deep circulation flow depth of 1 to 1.5 km depth, controlling stream chemistry and flow dynamics across the watershed.

Although EMMA has been successfully implemented in many studies, its application depends on selecting conservative tracers (Christophersen and Hooper, 1992; Hooper, 2003; Carrera et al., 2004; Barthold et al., 2011). Choosing conservative tracers is often challenging, mainly due to water-rock reactions and anthropogenic pollution affecting groundwater chemistry (Parkhurst, 1997; Carrera et al., 2004). The non-conservative behavior of species significantly decreases dataset size, reducing the representativeness of the groundwater system (Rueedi et al., 2015). To broaden the application of EMMA using non-conservative tracers, Pelizardi et al. (2017) combined non-conservative solutes to create conservative chemical components. The conservative components are created by defining the chemical system in a stoichiometric matrix, *S*. The *S* matrix contains the reactions, the species, and the stoichiometric coefficients. MIX estimates mixing ratios by using conservative species concentration while acknowledging uncertainty in end-member concentrations using a maximum likelihood method.

In the California Central Valley aquifer system, more than 75% of agricultural water supply derives from precipitation in the Sierra Nevada (Rosenthal and Dozier, 1996), and MSR from the Sierra Nevada constitutes a significant recharge component, 20% compared to 11% from diffuse recharge (Meixner et al., 2016). However, significant uncertainties exist in the Sierra Nevada's MSR estimates, and no information about groundwater flow paths from headwaters to the Central Valley aquifer system is available. Our objective is to address this critical knowledge gap by using multiple tracers and EMMA to characterize groundwater flow paths from the southern Sierra Nevada mountain aquifers to the northern Tulare basin in California's Central Valley and differentiate MFR, MBR, and VAR processes. The Tulare basin is one of the most over-drafted basins in California. Groundwater storage decreased by about 3 km^3/yr over the last decades (Alam et al., 2019), and the depletion rate was three times higher during the 2006-2010 and 2012-2016 droughts (Scanlon et al., 2012; Xiao et al., 2017). We used hydrochemical and isotope data from the US Geological Survey Groundwater Ambient Monitoring and Assessment (GAMA) program (Bennett et al., 2017) and implemented a multi-tool isogeochemical approach combined with EMMA and MIX analysis to answer three main research questions: 1) How does groundwater chemistry vary in the mountain-valley aquifer system of the northern Tulare basin? 2) How to differentiate MAR, MFR, and MBR processes using major chemical solutes and isotope tracers?, and 3) What is the hydraulic connectivity between the mountain and valley groundwater systems?

2. Materials and Methods

2.1. Study Area

The study area constitutes the northern Tulare Basin in California, with an area of 9,914 km2 extending between the Coastal Range in the west and the Sierra Nevada in the east. The area encompasses the Kaweah River, Tule River, and Tulare Lake watersheds (Figure 2a). Historically, the Tule River, Kaweah River, and the Kings River were discharging into the currently dry Tulare Lake. Elevation varies from 4421 masl on Mount Whitney to below sea level in the valley significantly impacting the climate. Lowlands (< 1,500 m elevation) and mid-elevation montane regions (1,500 – 2,500 m) have Mediterranean to semi-arid desert climate with hot and dry summers and cold winters (Boiano et al., 2005). Regions above 2,500 m elevation have Alpine climate with mean temperature lower than 10oC (Boiano et al., 2005). Mean annual precipitation varies between 150 mm in Lowlands to over 1000 mm at elevations above 2500 m, and mainly occurs from November to March (Faunt et al., 2016; NOAA, 2022).

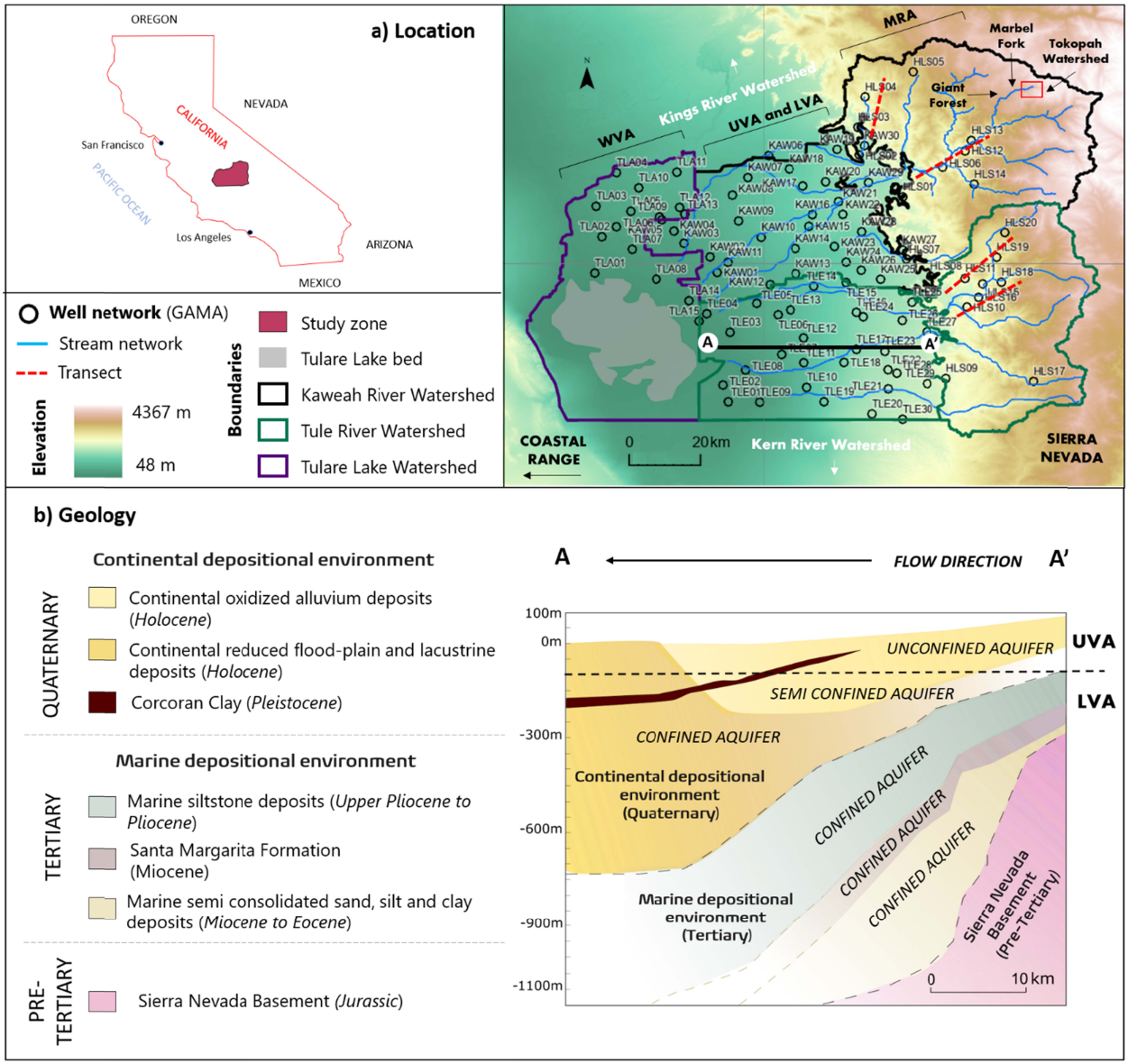

Figure 2. a) Location of the study area comprising the Kaweah River, Tule River, and Tulare Lake watersheds, GAMA network, and four regions defined in this study: Mountain Range Aquifer (MRA), Upper Valley Aquifer (UVA), Lower Valley Aquifer (LVA) and Western Valley Aquifer (WVA). b) Modified geologic cross section (A-A') from Lofgren and Klausing (1969) with the main hydrogeological units. Vertical exaggeration is x26.

2.2. Geology and Hydrogeology

The study region physiography consists of the Sierra Nevada in the east and the Central Valley. The Sierra Nevada comprises Jurassic granitic rocks, including granodiorite containing quartz, potassium feldspar, plagioclase feldspar, biotite, and hornblende (Huber, 1987). The Central Valley sedimentary basin mainly consists of Tertiary marine to Quaternary continental sediments deposited over a crystalline pre-tertiary basement. On the west, the study region is bounded by faulted sedimentary, volcanic, and metamorphic rocks of the Coastal Range (Lofren and Klausing, 1969) (Figure 2b). Six central Tertiary to Quaternary sedimentary units are identified

from bottom to top in the valley: (1) Marine semi-consolidated deposits (Tertiary), (2) the Santa Margarita Formation (Tertiary), (3) Marine siltstone deposits (Tertiary), (4) Lacustrine and flood-plain deposits (Quaternary), (5) Oxidized continental deposits (Quaternary), and (6) the Corcoran clay (Quaternary) (Figure 2b).

- The Marine semi-consolidated deposits with thicknesses between 60 m to 460 m are Miocene to Eocene age marine sand, silt, and clay sequence (Park and Weddle, 1959; Hilton et al., 1963). These layers behave as a confined aquifer and contain highly saline water (Lofren and Klausing, 1969).
- The Santa Margarita Formation (Diepenbrock, 1933) is a Miocene age marine unit with 50 m to 160 m thickness and mainly composed of fine gravel, fine to coarse sand, very fine green to gray clay, and shale facies (Hoots et al., 1954). This unit is the deepest freshwater aquifer in the study area used for agriculture (Lofren and Klausing, 1969).
- The marine siltstone Pliocene and Pliocene deposits with 190 m to 800 m thickness are siltstone diatomaceous deposits partially cemented by clayey siltstone interbedded with thin sand beds that contain saline water (Klausing and Lohman 1964). The overall transmissivity of the siltstone unit is exceptionally low.
- The late Pliocene to Holocene reduced clay, silt, and sand green to gray lacustrine and flood-plain deposits have maximum thicknesses of 1000 m in the west (Frink and Kues, 1954; Davis et al., 1959, Inter-Agency Committee 1958: Lofgren and Klausing, 1969). Plants and disseminated iron sulfide are well-preserved in them and their saline water is not suitable for drinking or agricultural uses (Lofgren and Klausing, 1969).
- The Holocene oxidized continental alluvial deposits are yellow to brown highly weathered sand, silt, and sandy clay feldspar grains (Frink and Kues, 1954; Davis et al., 1959, Inter-Agency Committee 1958: Lofgren and Klausing, 1969). The thickness of these highly weathered sediments is 90-200 m, and the unit is overlaid by 60-80 m of slightly weathered, highly calcareous permeable alluvial deposits. These calcareous deposits represent a time-lapse and a transition in the weathering regime (Lofgren and Klausing, 1969), and constitute the principal aquifer in the study area.
- The Corcoran Clay deposits are silty clay to clayey silt diatomaceous Pleistocene deposits occupying half of the study area in the western side. They are principal confining formation beneath the alluvial deposits and flood plain with thicknesses ranging from 0 m in the east to more than 30 m in the west (Lofgren and Klausing, 1969).

The regional groundwater flow is from east to west, following the Sierra Nevada streams. The oxidized alluvial deposits form the principal unconfined aquifer in the eastern part of the study area transitions to semiconfined and confined aquifers in the west because of the Corcoran Clay. In the east, the saline water has naturally been replaced by fresh water forming a secondary confined aquifer in the Santa Margarita Formation. The low-quality high salinity groundwater is in the western part of the confined Pliocene sediments aquifer and the confined Santa Margarita Formation aquifer (Lofgren and Klausing, 1969).

2.3. Hydrochemical and Isotopic Data

We used hydrochemical and isotopic data from domestic wells sampled as part of the US Geological Survey (GAMA) Program (Bennett et al., 2017). The dataset includes 95 wells sampled from November 2014 to April 2015. Among multiple groundwater-quality parameters,

we used pH, temperature (T), alkalinity, major ions (Ca, Mg, Na, K, Cl, SO_4), NO_3, Br, stable isotopic ratios of hydrogen (^2H), oxygen (^{18}O), and carbon (^{13}C), and tritium (^3H). The quality criterion for the chemical analyses was cation-anion imbalances of ≤ 10%. Unfortunately, only 40% of the wells (41 wells) had ion imbalance errors of smaller than 10%, and the remainder (54 wells) had higher errors and were discarded from the chemical analysis. These 54 wells were included for pH, temperature, stable hydrogen (^2H), oxygen (^{18}O), and tritium (^3H) analysis. Rainwater isotopic content was obtained from previous studies in California (Visser et al., 2018; Friedman et al., 1992; Rose et al., 1996). Meltwater isotopic signatures were from a 2-year study in the Marble Fork of the Kaweah (Figure 1a) watershed (Huth et al., 2004).

The studied groundwater system was divided into four aquifer regions. The Mountain Range Aquifer (MRA) includes 18 wells at 181 to 876 m elevations with depths varying from 30 to 182 m. The Upper Valley Aquifer (UVA) comprises the unconfined regions of the Central Valley aquifer and includes 37 wells at elevations from 61 to 149 m and depths of less than 100 m (17-98m). The Lower Valley Aquifer (LVA) comprises the semi-confined to confined areas of the Central Valley aquifer and includes 23 wells with depths greater than 100 m (107-453 m) and elevations from 64 to 214 m. The 100 m separation depth for differentiating UVA from the LVA was based on the geological cross-section A-A' (Figure 2a) of Lofgren and Klausing (1969) and was confirmed by a recent large-scale geophysical investigation (Kang et al., 2022). This division was not applied to the Western Valley Aquifer (WVA) wells close to the historical Tulare Lake. Elevation of the 15 WVA wells ranges from 66 to 81 m, with depths from 24 to 91m. Nearly all shallow wells are pumping fresh water from the continental oxidized alluvial deposits. Only WVA and western LVA wells are extracting water from the continental lacustrine deposits. Eastern LVA wells are pumping freshwater from saline Tertiary deposits which saline formation water has been flushed out.

2.4. Isogeochemical Analysis and Modeling

2.4.1. Characterizing Chemical and Stable Carbon (^{13}C) Isotopic Signatures of the Mountain-Valley Aquifer system

We employed a multi-tool approach using hydrochemical data to determine groundwater chemical facies of aquifers. After identifying temperature and pH ranges of wells, groundwater chemical facies were determined by Stiff diagrams. The potential processes driving each facie were determined using a Piper diagram and later validated using multiple approaches. The influence of evaporation and cation exchange processes were evaluated using two models built in PHREEQC version 3 (Parkhurst & Appelo, 2013). In the first model, evaporation was the main process driving dissolved cations in the MRA. The evaporation effect was assessed by calculating a concentration factor (C_f) using the Giant Forest Rain station data in the Kaweah River watershed (Figure 2a) (NADP, 2022). Assuming Cl was conservative, the C_f was obtained by comparing the average Cl concentrations in the MRA groundwater and volume-weighted precipitation accounting for wet and dry deposition from the 1980-2020 period. In the second model, evaporation and cation exchange were considered. The average exchangeable base concentrations were obtained using soil information from two sites in the Tokopah Watershed located in the Kaweah River basin (Figure 2a) (Table S1). The average exchangeable base concentrations were converted from meq/100g to eq/kg using sediment porosity of 0.45 and soil bulk density of 2.6 g/cm^3. Exchange equilibrium constants were from Appelo & Postma (2005) following the Gaines-Thomas convention. The plausibility of both models was assessed by

comparing the estimated dissolved cations concentrations to the average measured concentration in the MRA.

While evaporation and cation exchange primarily relate to soil driven processes within the unsaturated zone, groundwater chemistry is highly influenced by mineral dissolution and precipitation processes. These processes were evaluated using mineral saturation indices (SI). SI indicates how far groundwater is from the mineral equilibrium and determines the dissolution or precipitation potential of a specific mineral. SI was computed with PHREEQC using in-situ temperature, pH, and alkalinity measurements. Mineral equilibrium was assumed within ± 0.5 of SI. Complementary to the SI, mineral dissolution was assessed by bivariate analysis of groundwater dissolved solutes. The bivariate analysis of reaction products is instrumental when dissolution and precipitation processes cannot be identified by the SI. For example, as silicate dissolution is slow, silicates are expected to be far from equilibrium indicating sub-saturation. In addition, silicates are usually altered to other minerals with a different chemical structure and composition. A well-known example is weathering of the Sierra Nevada granite studied by Feth et al. (1964) and Garrels and McKenzie (1967). In these studies, granite silicates including andesine $Na_{0.62}Ca_{0.38}Al_{1.38}Si_{2.62}O_8$, K-feldespar and biotite $KMg_3AlSi_3O_{10}(OH)_2$ were altered to kaolinite $Al_2Si_2O_3(OH)_4$, releasing Na^+, Ca^{+2}, K^+, HCO_3^- and SiO_2 as follows:

$$1.77Andesine + 2.44CO_2 + 3.67H_2O \rightarrow 1.23Kaolinite + 1.10Na^+ + 0.68Ca^{2+} + 2.44HCO_3^- + 2.20SiO_2 \quad \text{Eq. 1}$$

$$0.13K - feldespar + 0.13CO_2 + 0.195H_2O \rightarrow 0.065Kaolinite + 1.13K^+ + 0.13HCO_3^- + 0.26SiO_2 \quad \text{Eq. 2}$$

$$0.037Biotite + 0.51CO_2 + 0.26H_2O \rightarrow 0.037Kaolinite + 0.073K^+ + 0.22Mg^{2+} + 0.51HCO_3^- + 0.15SiO_2 \quad \text{Eq. 3}$$

Bivariate analysis was fundamental to understand water-rock reactions in the aquifer systems. Moreover, it was used to identify: (1) pollution from the agriculture fields through the NO_3-SO_4 relation, and (2) seawater mixing from the Tertiary marine deposits through the Na-Cl and SO_4-Cl relations.

2.4.2. Characterizing MSR Processes with Stable Oxygen (^{18}O) and Hydrogen (^{2}H) Isotopes and Tritium (^{3}H)

Stable ^{18}O and ^{2}H groundwater isotopes were used to differentiate focused from diffuse MAR in the MRA wells. Focused MAR mainly occurs via streamflow infiltration and seepage from lakes through the mountain block, and groundwater samples are expected to express isotopic fractionation due to evaporation. Stable isotopic data from the evaporated MRA wells representative of focused MAR in the Sierra Nevada were used to build a Local Evaporation Line (LEL). To identify recharge sources (rain, snowmelt, and surface water) in the MRA wells, stable isotopic values of fourteen MRA wells located in four different transects across the elevation gradient (Figure 2a) were used.

The MFR was attributed to shallow wells at the mountain front with the isotopic signature of evaporated Sierra Nevada rivers (focused MAR) and the chemical signature of unsaturated zone processes. The deep MBR was attributed to deep wells with the chemical signature of water-granite reactions and long residence times (tritium concentrations are ≤0.5 tritium units (TU)).

2.4.3. Quantifying the Connectivity between the Mountain and Valley Groundwater Systems

The proportion of MFR and MBR in valley aquifer wells was computed using the (1) End-Member Mixing Analysis (EMMA) (Christophersen and Hooper, 1992; Hooper, 2003) and (2) mixing ratio calculation (MIX) (Carrera et al., 2004). EMMA is based on the principal component analysis, aiming to find the composition and a minimum number of end-members needed to explain the variability of measured concentrations within water samples. MIX calculates the mixing ratios of the identified end-members in each sample using the concentrations of conservative species. A detailed description of MIX can be found in Carrera et al. (2004), and a summary is provided below. The mass balance equation of a sample (mixture) p for species s is defined as (Carrera et al., 2004):

$$y_{ps} = \sum_{e-1}^{ne} \delta_{pe} x_{es} + \varepsilon_{ps} \qquad where\ s = 1, \dots, ns \qquad \text{Eq. 4}$$

Where y_{ps} and x_{es} are the concentrations of species *s* in sample *p* and end-member *e*, respectively, δ_{pe} is the proportion of end-member *e* in mixture *p*, and ε_{ps} accounts for measurement and conceptual errors caused by the non-constant concentration of an end-member. When the end-member concentrations are known, the errors in simulated concentrations can be calculated using an objective function.

Correct application of EMMA and MIX requires selection of conservative species, and end-members with significant differences in species concentrations (Christophersen and Hooper, 1992; Hooper, 2003; Carrera et al., 2004; Barthold et al., 2011). As achieving conservative condition due to water-rock reactions in groundwater is challenging (Parkhurst, 1997; Carrera et al., 2004), we followed the Pelizardi et al. (2017) approach by linearly combining non-conservative species with conservative chemical components. Components are linear combinations of species that remain unchanged by reactions. For example, the component $U_{gypsum} = Ca^{+2} - SO_4^{-2}$ will not change by gypsum dissolution (Eq. 5), and the exact amount of Ca^{+2} and SO_4^{-2} release by gypsum dissolution is predicted by:

$$CaSO_{4(s)} \leftrightarrow Ca^{+2} + SO_4^{-2} \qquad \text{Eq. 5}$$

Therefore, subtracting the molar concentration of SO_4^{-2} from Ca^{+2} will always give the same result, maintaining U_{gypsum} constant. In order to build chemical components, the chemical reactions and species must be defined in a stoichiometric matrix (Eq. 6), and components are built following Eq. 7.

$$S = N_r \times N_s \qquad \text{Eq. 6}$$

$$U = (N_s - N_r) \times N_s \qquad \text{Eq. 7}$$

Where S is the stoichiometric matrix containing the stoichiometric coefficients of the reactions, N_r is the number of reactions, N_s is the number of species, and U is a component. A detailed description of the component and stoichiometric matrices can be found in Molins et al. (2004) and Pelizardi et al. (2017), respectively. We also used components to validate processes

identified in Section 2.4.1. In EMMA, changes in species concentrations are presented via eigenvectors. Therefore, an eigenvector accounts for gypsum dissolution would contribute to Ca^{+2} and SO_4^{-2} in the same direction, either positive or negative, and the contribution will be the same due to the stoichiometry of Eq. 1 and range from 0 to 1. In general, more eigenvectors explain more variance of the sample composition as more species are considered.

In this study, end-members are representative samples of each main chemical groundwater type associated with MSR processes. A number of EMMA models were developed using different end-members, solutes, isotope tracers, and chemical reactions. The variance, R^2, and root mean squared error (RMSE) were jointly used to determine the best model (i.e., the model with the highest variance and the best fit between measured and modeled concentrations). Slope (m) identified the direction of those differences. Finally, the best-performing EMMA model was selected to run with MIX to obtain the percentage of MSR processes in each well, and quantify the connectivity between the mountain and valley groundwater.

3. Results and discussion

3.1. Characterizing Chemical and Stable Carbon (^{13}C) Isotopic Signatures of the Mountain-Valley Aquifer system

The average groundwater temperature in the study area is 20°C. Temperature ranges are 17 – 23°C (average = 20°C) in the MRA wells, and the UVA wells, 19 – 28°C (average= 23°C) in the LVA wells, and 19 to 23°C (average= 20°C) in the WVA wells. Only the LVA samples are three degrees warmer than the average groundwater temperature (Figure 3c). pH ranges in the MRA are 6.1 to 7.8 (average = 6.9), 6.9 to 8.5 (average= 7.6) in the UVA wells, 7.1 to 8.4 (average= 8.0) in the LVA wells, and 7.2 to 9.1 (average= 7.7) in the WVA wells (Table S1). On average the MRA wells (pH= 6.9) have lower mean pH than the study area average (pH= 7.7), indicating newly recharged groundwater with pH values closer to the average rainwater (pH ~ 5.5 for the 1980-2020 period). The LVA samples have a slightly higher pH and temperature (on average 3°C warmer than other regions) suggesting longer residence time.

Stiff diagrams indicate the presence of two major and three minor chemical facies (Figure 3a). Major groundwater types are Ca-HCO_3 and Na-HCO_3 as HCO_3 is the dominant anion of the entire dataset. In some samples (n=6, Figure 3a) SO_4 and HCO_3 are similar, leading to the minor chemical facie Na-HCO_3SO_4. Higher dissolved Cl concentration relative to HCO_3 in five samples results in two additional minor chemical facies, Na-Cl and Ca-Cl groundwater types. These wells are KAW04 in the UVA, TLE03 in the LVA, and TLA13, 14, and 15 in the WVA (Figure 3a). Cl only increases in a few samples (arrow c in Figure 3b) suggesting the influence of local processes driving Cl concentration. In contrast, SO_4 increases without exceeding HCO_3 (arrow *b* in Figure 3b) in all the aquifer regions except the MRA suggesting the role of regional processes on SO_4 concentrations.

Regarding the cations, the Ca-HCO_3 groundwater type dominates MRA and UVA regions except for 1 out of 10 (HLS14, Figure 3a), and 5 out of 16 Na-dominated samples. In the LVA and WVA regions, groundwater has evolved to Na-HCO_3 except for 4 out of 12 Ca-dominated samples in the LVA, and one Ca-Cl sample in the WVA (TLA13, Figure 3a). The Ca-HCO_3

evolved to Na-HCO_3 (arrow (a) in Figure 3b) while sulfate increases (arrow (b) in Figure 3b) suggesting the role of regional processes on groundwater evolution.

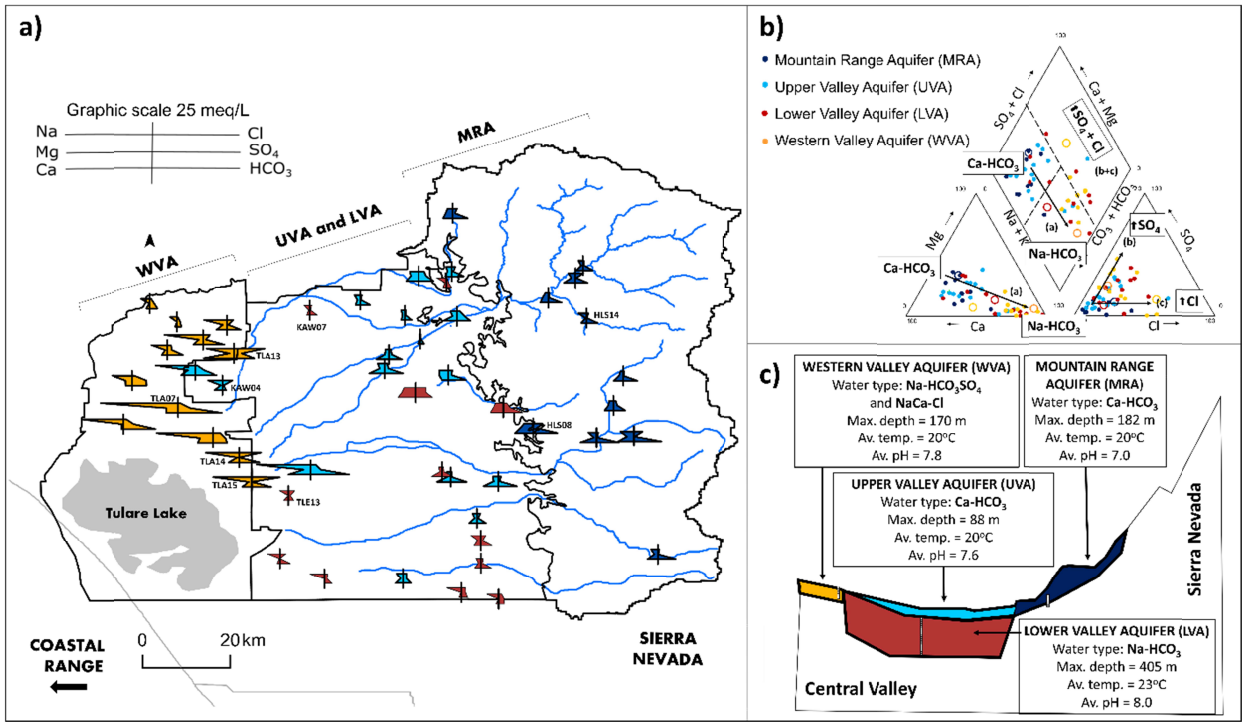

Figure 3 a) Spatial distribution of the Stiff diagrams. Each groundwater region is presented with a different color (MRA: dark blue, UVA: light blue, LVA: red, WVA: orange). B): Projection of the major chemical component of groundwater samples on a Piper diagram. Arrows highlight the main observed trends in groundwater chemistry. The empty circles are the selected end-members for the MIX analysis. C) Main hydrochemical features of each groundwater region.

3.1.1. Processes Driving the Major Ion Evolution in the Mountain-Valley Aquifer Regions

Mountain Range Aquifer

The Ca-HCO_3 groundwater type of the MRA was previously reported for the vast majority of Sierra Nevada rivers and lakes (White et al., 1999; Melack et al., 1985; Melack et al., 2020). This similarity with the surface water chemistry and rainwater pH suggests that the Ca-HCO_3 groundwater type represents newly recharged groundwater in the Sierra Nevada and its chemistry is likely influenced by soil-related processes such as evaporation and cation exchange. To evaluate this hypothesis two models that consider evapoconcentration and cation exchange processes are developed (Table 1). Model A accounts for increases in dissolved solutes due to evaporation and computes a concentration factor (C_f) using the rainwater and MRA samples by assuming Cl as a conservative solute. The ratio of average Cl concentration in the MRA (34.3 mg/L) and rainfall (0.11 mg/L) results in C_f of 311. The high evapoconcentration factor agrees with the significant mean evapotranspiration rate for the 1982-2019 period in the Mountain Range (639 mm/yr) (Elnashar et al., 2020) accounting for 84% of the average rainfall (756 mm/y) for the same period (NOAA, 2022). Model B considers evaporation and cation exchange processes using the averaged cation exchange capacity (CEC) of two soil types (1.19×10^{-4} eq/kgw) in the Tokopah watershed (Figure 2a), the exchange equilibrium constants from Appelo & Postma (2005), and following the Gaines-Thomas convention. Model results indicate that the

amount of cations released in Model B is less than Model A that only considers evapoconcentration. However, evapoconcentration only accounts for 40% of dissolved Ca in MRA groundwater, and other processes such as calcite dissolution and silicate weathering should be considered.

Table 1. Average chemical composition of the volume-weighted average rainfall at the Giant Forest Rain station during the 1980-2020 period (first row), and average cation and Cl concentrations in the MRA region (mg/L). Calculated cation and Cl concentrations from Model A and B by considering evapoconcentration, and evapoconcentration and cation exchange processes, respectively.

	Ca	Mg	K	Na	Cl
VWA Rainfall (1980-2020)	0.05	0.01	0.02	0.06	0.11
Mean MRA samples	60.0	16.8	4.2	39.10	34.30
Model A – Evapoconcentration	14.36	3.52	5.79	19.91	34.30
Model B – Evapoconcentration + Cation Exchange	10.96	2.05	9.17	24.59	34.30

The contribution of calcite dissolution to Ca concentration in surface water bodies and shallow groundwater in the Sierra Nevada is controversial. Some studies demonstrated that more than half of Ca in surface water is released by calcite dissolution (Mast et al. 1990; Clow et al. 1997). A recent study also showed that isolated small karst systems in the Sequoia National Park contribute to 65-86% of baseflow in the North and East Fork of the Kaweah River during the dry season, leading to increases in Ca (Tobin and Schwartz, 2020). White et al. (1999) attributed Ca concentration in the Northern Sierra Nevada groundwater to accessory calcite in fresh granitoid rocks, and Garrels and Mackenzie (1967) attributed 70% of Ca variability in the perennial springs to calcite dissolution and the remainder to evapoconcentration. Other studies indicated that silicate weathering is the main source of Ca (Feth et al., 1964; Wahrhafting, 1965; Melack et al., 2021; Williams et al., 1990; Williams et al., 1993). Among the main Sierra Nevada granodiorites, andesine, quartz, K-feldspar, and biotite, only andesine has the potential to release Ca in groundwater (Feth et al., 1964; Garrels and Mackenzie, 1967; Sisson et al., 1984; Clow et al., 1996). However, andesine weathering cannot solely explain high Ca concentration. Andesine has a molar Ca/Na ratio of <1. Figure 3a shows that Na increases due to andesine weathering are associated with decreases in CO_2 as expected by Eq. 2. (Table S2). Ca/Na ratio of surface water and shallow groundwater of the Sierra Nevada is greater than 1, so andesine is the primary source of Na.

Although andesine is the most prevalent silicate in the Sierra Nevada, biotite is the most easily weathered silicate, and about 1%-2% of the biotite is altered to clay minerals (Wahrhafting 1965; Meade 1967). Therefore, biotite weathering and evaporation are the likely sources of dissolved Mg in groundwater (Eq. 6), and silicate weathering and calcite dissolution are sources of Ca and Na in the MRA groundwater. Silicate weathering and calcite dissolution reactions also account for groundwater alkalinity as shown by the HCO_3 release in Eq.1, Eq.2, Eq.3, Eq.4, and Eq.8.

$$CaCO_3 + CO_2 + H_2O \leftrightarrow Ca^{+2} + 2HCO_3^- \quad \text{Eq. 8}$$

In summary, andesine is the primary source of Na in the MAR, and biotite and evaporation are the sources of Mg. The primary source of K seems to be evaporated rainfall, even though biotite

could also contribute. Calcite dissolution releases part of the dissolved Ca and HCO_3 in groundwater, and jointly with silicate weathering contribute to dissolved HCO_3. In agreement with the previous investigations, most of the MRA groundwater samples are in equilibrium with calcite except for a few sub-saturated samples (Figure 3b).

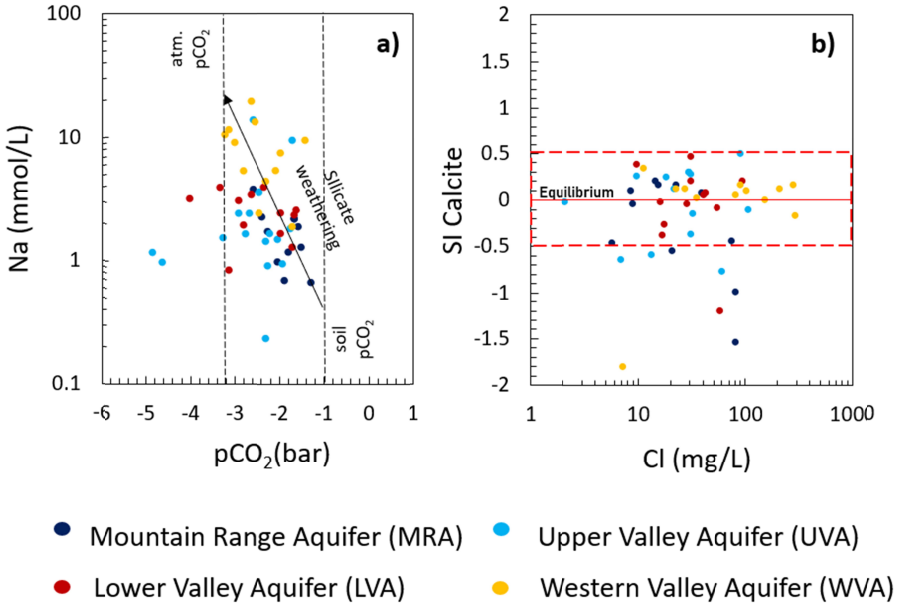

Figure 4. a) Relation between dissolved Na (mmol/L) and dissolved edaphic CO_2 (pCO_2 bar); b) Relation between the SI of calcite ($CaCO_3$) and dissolved Cl (mg/L).

Valley Aquifer System

The valley area comprised of UVA, LVA, and WVA groundwater regions. Due to low precipitation in the valley area, valley groundwater is mainly recharged by MFR and MBR processes originating from the mountain and influencing groundwater chemistry of the valley (Figure 1).

The Ca-HCO_3 chemical facie of the MRA is also dominant in the UVA region, and highly calcareous alluvial sediments of the UVA (Lofgren and Kalusing, 1969) support calcite dissolution. Calcite equilibrium is achieved in most of the UVA samples (Figure 4b), and calcite equilibrium in the less mineralized samples suggests that the Ca-HCO_3 groundwater type is influenced by soil processes, and rivers and lakes chemistry. The similarity between the MRA and UVA samples implies that unsaturated zone processes impact recharge chemistry.

The main differences in the groundwater chemical composition between the MRA, UVA (Ca-HCO_3), and LVA (Na-HCO_3) is the Na dominance among other cations and decreases in dissolved Ca and HCO_3 in the LVA region. The Na dominance suggests strong influence of andesine weathering over calcite dissolution and cation exchange. Andesine weathering is a slow process where thermodynamic equilibrium is rarely attained (Appelo & Postma, 2005). Therefore, long water-rock contact and residence time result in the Na-HCO_3 chemical type. This hypothesis also agrees with the low mineralization of the deepest wells in the LVA (i.e., smaller Stiff diagrams in Figure 3a) region and warmer temperature of the LVA samples due to geothermal characteristics of deep flow circulation (Figure 3c).

The WVA chemical composition is very similar to the LVA but more mineralized (Figure 3a). The most prevalent solutes in the WVA are Na, HCO_3, SO_4, and Cl (Table S1), resulting from similar water-rock reactions. More mineralization compared to the LVA is consistent with a longer distance from the recharge area (Figure 3c). Another major difference between these regions is the local dominance of Cl over HCO_3. Fuji and Swan (1995) attributed the Cl increase to the influence of Miocene marine sedimentary rocks derived from the Coast Range, seawater mixing, salts dissolution, and evaporative processes. We developed a binary mixing model to explore the possible mixing of fresh groundwater with seawater (Figure 5a). The less mineralized MRA Ca-HCO_3 groundwater sample was selected as the representative freshwater end-member, and the chemical composition of standard seawater was obtained from Hem (1985). The short distance of Na-Cl and Ca-Cl WVA labeled samples from the mixing line suggests that seawater mixing is the main contributor to dissolved Cl (Figure 5a). In Fuji and Swan (1995), evaporation and dissolution of evaporative salts were supported by the observed salt crusts in soils of non-irrigated fields. Salt dissolution potential due to evaporative processes was evaluated by plotting the SI of halite (NaCl) versus Cl (mg/L) (Figure 5b). Results show sub-saturation of halite in all samples, eliminating salt dissolution as the Cl source. Therefore, the dominant processes driving the high mineralization of the WVA region and the local increase in dissolved Cl are prolonged water-rock interactions promoting silicate weathering and mixing with seawater from the Quaternary lacustrine and flood-plain deposits.

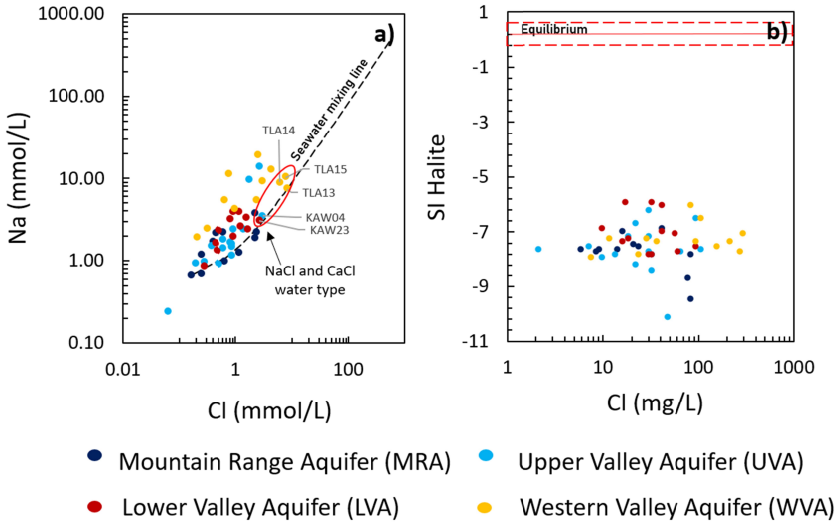

Figure 5. a) Relation between dissolved Na and dissolved Cl (mmol/L). b) Relation between the SI of halite (NaCl) and dissolved Cl (mg/L).

3.1.2. Assessing Sulfate Sources in Groundwater Samples

In all aquifer regions, increases in sulfate are observed (arrow (b) in Figure 3b). The WVA samples have higher dissolved SO_4 concentrations, on average 50 to 85 mg/L more than the other aquifer regions (Table S1). Three potential processes were assessed to explain dissolved SO_4 sources: (1) agricultural or sewage contamination, (2) mixing with seawater trapped in the Quaternary and Tertiary sediments, and (3) gypsum dissolution. Agricultural or sewage pollution impact groundwater via direct infiltration of excess fertilizer. Nitrate concentrations in shallow domestic wells in the Central Valley are derived from multiple anthropogenic sources (manure, synthetic fertilizer, and septic/wastewater discharge) (Moran et al., 2011). Therefore, a strong

linear relationship between SO_4-NO_3 will suggest SO_4 anthropogenic pollution. However, no correlation (R^2=0.01) between the SO_4 and NO_3 concentrations is found eliminating anthropogenic sources for SO_4 (Figure 6a).

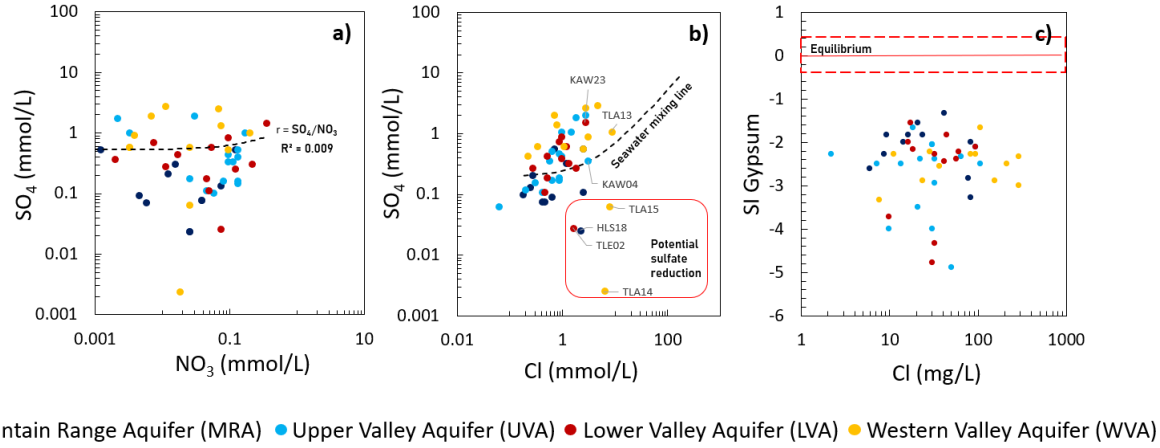

Figure 6. a) Relation between dissolved SO_4 (mmol/L) and dissolved NO_3 (mmol/L). b) Relation between dissolved SO_4 and dissolved Cl (mmol/L). Labeled samples are Na-Cl, Ca-Cl groundwater type. C) Relation between the SI of gypsum ($CaSO_4$) and dissolved Cl (mg/L).

Seawater mixing was evaluated through the mixing model. Most groundwater samples including the Na-Cl dominated samples (labeled samples in Figure 6b) are plotted higher than the Cl-SO_4 seawater mixing line indicating higher dissolved SO_4 than expected by the seawater mixing (Figure 6b). Higher SO_4 concentrations in KAW23 and TLA13 samples are related to gypsum dissolution. The Ca-Cl samples have lower SO_4 values than expected by the seawater mixing, potentially due to sulfate reduction processes. Only KAW04 sample seems to be affected by the seawater mixing. Therefore, even if seawater mixing is responsible for higher dissolved SO_4 in some samples, other processes are the main drivers of SO_4 concentration in groundwater.

Gypsum dissolution was evaluated by computing the gypsum Saturation Index (SI_{gypsum}). Results shows that all groundwater samples are sub-saturated. Saturation indices of the MRA samples are higher than average (average SI_{gypsum}=-2.1) (Table S2), but small differences are observed among the UVA (SI_{gypsum}=-2.8), LVA (SI_{gypsum}=-2.7), and WVA (SI_{gypsum}=-2.5) samples (Table S1). Feth et al. (1964) reported sulfate nearby fault zones in the Sierra Nevada. In addition, Lofren and Klausing (1969) and Meade (1967) reported sulfate and ion sulfides in the Quaternary sediments. Petrographic evidence suggests that part of the sulfate from the iron sulfide oxidation reacts with calcite forming gypsum in the Quaternary sediments (Meade 1967). The absence of chloride in sediments agrees with our results that the SO_4 increase is not followed by a dissolved Cl increase (Figure 6b). Although gypsum equilibrium is not observed in our samples, gypsum dissolution is likely to occur locally at the fault zones and valley sediments explaining the wide range of dissolved SO_4 in groundwater. However, sulfur isotope analysis is needed to confirm this hypothesis.

The evolution of δ^{13}C-HCO_3(‰) in groundwater is used to evaluate the gypsum dissolution hypothesis. Gypsum dissolution ($CaSO_4$) increases dissolved Ca without changing δ^{13}C (‰) content in groundwater. However, calcite ($CaCO_3$) dissolution results in less depleted δ^{13}C (‰) values (i.e., δ^{13}C of calcite is close to 0 ‰).

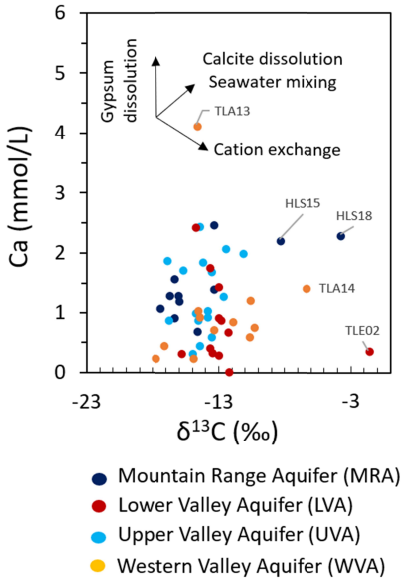

Figure 7. Relation between dissolved Ca (mmol/L) and $\delta^{13}C$ (‰).

Results in Figure 7 confirm that gypsum dissolution drives dissolved Ca concentration in groundwater as groundwater samples follow the gypsum dissolution direction, with some samples having exceptionally high dissolved Ca. The $\delta^{13}C$ (‰) of dissolved inorganic carbon in groundwater samples ranges from -17.16 ‰ to -10.40 ‰, excluding those with anomalous values HLS15, TLA14 HLS18, and TLE02 samples (-8.4‰ < $\delta^{13}C$ < -1.68 ‰). Dissolved inorganic carbon in the above samples with larger $\delta^{13}C$ (‰) values is usually the result of organic matter oxidation. In this case, sulfate reduction is likely oxidizing the organic matter and driving increases in $\delta^{13}C$ values due to the low dissolved SO_4 (Figure 6 and Table S2). Additionally, calcite dissolution locally enhanced by Ca-Na cation exchange seems responsible for the $\delta^{13}C$ of -17.16‰ to -10.40 ‰ in groundwater. $\delta^{13}C$ of a groundwater system in equilibrium with calcite would range from -16‰ to -12‰. However, some samples have larger $\delta^{13}C$ values due to Ca-Na cation exchange and oversaturation. Finally, gypsum and calcite dissolution are regional processes driving the dissolved Ca, SO_4 and HCO_3 in groundwater and oxidation of organic matter and cation exchange only have local effect.

3.2. Characterizing Chemical and Isotopic Signatures of MSR processes with Stable Oxygen (^{18}O) and Hydrogen (^{2}H) isotopes and Tritium (^{3}H)

Groundwater $\delta^{2}H$ and $\delta^{18}O$ values from all four groundwater regions are plotted along the Global Meteoric Water Line (GMWL; Craig, 1961). The isotopic content of the samples ranges from -51.1‰ to -97.4‰ for $\delta^{2}H$ and -5.68‰ to -13.59‰ for $\delta^{18}O$ (V-SMOW) (Figure 8a). A Local Evaporation Line was determined from the MRA region samples (Figure 8a), and its slope agrees with the US rivers (Kendall & Coplen, 2001; Mast et al., 1990).

The slope of the topographic fractionation effect in California ranges from -1.7 to -2.7 ‰ per vertical km for $\delta^{18}O$ ‰ (Friedman, 1992; Rose et al., 1996; Lechler et al., 2012; Visser et al., 2018). However, comparing the expected topographic fractionation with the isotopic composition of samples along the elevation transects (Figure 2a) indicates a different response. While the estimated topographic fractionation effect is 1.15‰ between the $\delta^{18}O$ values of T1 and

T4 wells (1062 – 386 = 676 m altitude difference, Figure 8b), the observed difference is 0.42‰ (Figure 8b). This result highlights the importance of snowmelt processes in controlling the isotopic composition of meltwater. Accordingly, the $\delta^{18}O$-$\delta^{2}H$ isotopic space was divided by the precipitation type: rainwater versus meltwater while considering different stages of snowmelt. Rainwater isotopic content was obtained from previous studies in California (Visser et al., 2018; Friedman et al., 1992; Rose et al., 1996). Meltwater signatures were from a 2-year study in the Marble Fork (Figure 1a) watershed indicating $\delta^{18}O$ ranges of -16‰ to -14‰ for the initial meltwater and -11‰ to -10‰ for the final meltwater (Huth et al., 2004) (Figure 8a).

The oxygen and hydrogen isotope composition of the MRA wells seems to be influenced by fractionation during snowmelt and evaporation, except for the only Na-HCO_3 and non-evaporated MRA sample (HLS14) (Figure 3a). Isotopic values of MRA wells follow the LEL ($\delta^{18}O$ values range from -9.82‰ to -5.68‰) are representative of focused MAR and are comprised of rainwater and final meltwater.

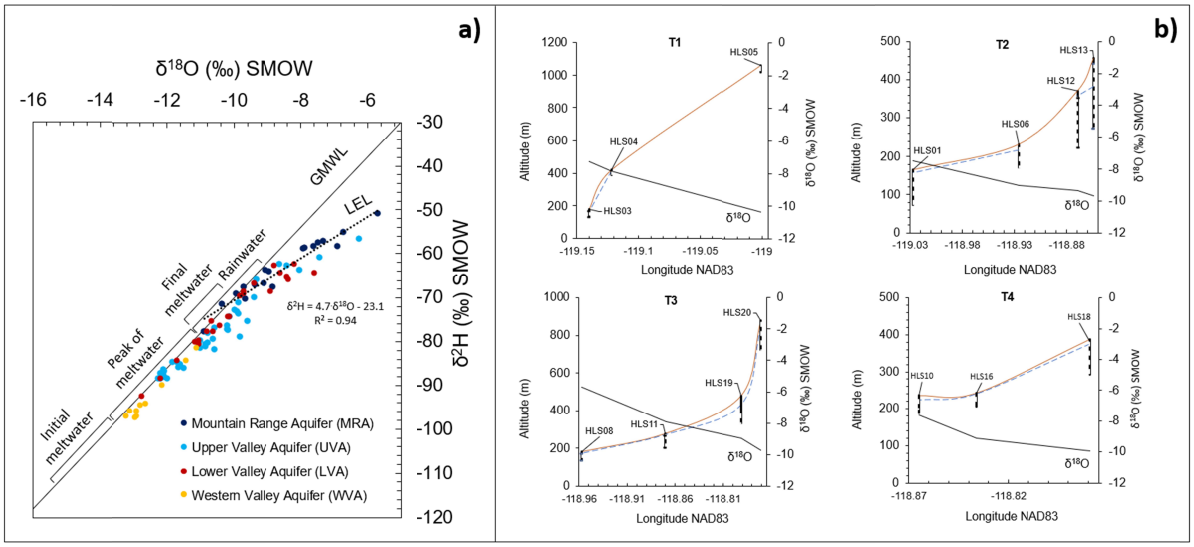

Figure 8. a) $\delta^{2}H$ and $\delta^{18}O$ content in groundwater. Global Meteoric Water Line (GMWL; Craig (1961)) and Local Evaporation Line ($\delta^{2}H$ =4.6$\delta^{18}O$ -23.3). Initial and final meltwater isotopic ranges are from Huth et al. (2004). Rain isotopic values are from Visser et al. (2018), Friedman et al. (1992) and Rose et al. (1996). B) Altitude of wells (orange line), groundwater level (discontinuous blue line), well (black line) and screen depth (discontinuous black line), and $\delta^{18}O$ values of four MRA transects.

The evaporation signature jointly with the Ca-HCO_3 groundwater type, characteristic of surface water bodies, are used to identify MFR. UVA groundwater samples located at the mountain front or close to the Kaweah River follow the LEL (KAW18,19,25,26,28,29; TLE23,25,27, Figure 2a) and are Ca-HCO_3 type (Figure 3a) indicating MFR influence. The non-evaporated Ca-HCO_3 UVA samples influenced by soil processes, represent diffuse MAR and shallow MBR recharging the first 100 m of the unconfined aquifer. The LVA groundwater samples from the deeper wells (depth > 150 m) close to the mountain front (TLE20, 22,29,30 Figure 2 and Table S1) also follow the LEL and are mostly Na-HCO_3 groundwater type indicating the influence of focused MAR and deep MBR processes. Non-evaporated LVA and all WVA samples following the GMWL represent diffuse MAR and deep MBR processes, and their isotopic signatures indicate the influence of meltwater recharge during the peak of snowmelt (days 170 – 210 of the water year).

To further confirm the long residence time of MBR recharging the confined aquifer groundwater tritium (^3H) content was used. Tritium has a half-life of 12.5 yr. implying complete decay (i.e., tritium units (TU) = 0) after 50 years. Groundwater ^3H content ranges from 20 to 0 TU (Table S1). The LVA and WVA samples from wells with depths greater than 150 m have 0 TU (Figure 9) and are Na-HCO_3 with the exception of Ca-HCO_3 LVA sample (TLE21). These results agree with Visser et al. (2016) that predict 3 to 0 TU in California wells with depths greater than 122 m. Wells with depths greater than 150 m and residence times longer than 50 years that contain evaporated Na-HCO_3 groundwater type are recharged by focused MAR. This result highlights the contribution of mountain rivers and lakes to confined aquifer recharge. LVA wells with more than 0 TU that have long-screens with the screen top in the unconfined aquifer (Table S1) are the result of mixing with shallower young groundwater. Five UVA wells with depths less than 150 m (samples TLA14, KAW12, TLA03, KAW09, and TLE09) have also 0 TU and are Na-HCO_3 indicating shallow MBR recharge with long residence time. Shallow MBR is a result of complex geology of mountain ranges and presence of faults and fractures impacting flow direction.

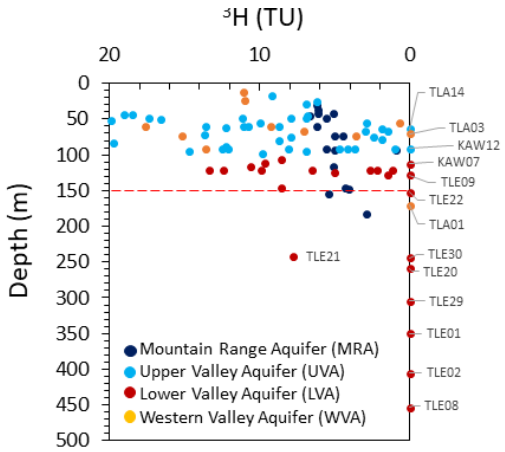

Figure 9. Tritium (Tritium Units, TU) content in groundwater samples in the study.

In summary, rain and meltwater are sources of recharge. The oxygen and hydrogen isotopic composition of the MRA groundwater is highly influenced by meltwater processes rather than the topographic isotope effect, and focused MAR is the dominant recharge process. Focused MAR is the evaporated Ca-HCO_3 water type that recharges the first 100 m of the upper valley aquifer and along with evaporated Na-HCO_3 also contributes to deep MBR in the confined aquifer (Figure 10). As a result, groundwater chemistry at the piedmont zone is influenced by focused MAR discharging to valley aquifer and focused MFR from mountain streams. Meltwater from diffuse MAR either becomes Ca-HCO_3 water and contributes to shallow MBR in the UVA region (Figure 10), or infiltrates though the saprolite layer, faults and joints, and recharges the deeper aquifer and becomes Na-HCO_3 water type that contributes to deep MBR in the LVA and WVA regions (Figure 10). The shallow MBR zone near the foothills represents a mixing zone that consists of Na-HCO_3 water type from the LVA region and Ca-HCO_3 water type from the UVA region (Figure 10). Evapotranspiration, calcite dissolution, and biotite weathering are responsible for the Ca-HCO_3 groundwater, and andesine weathering is responsible for the Na-HCO_3 groundwater type. The Na-HCO_3SO_4 groundwater type is associated with deep MBR and prolonged exposure to silicate weathering and gypsum dissolution in the western region of the

upper aquifer. The NaCl and CaCl groundwater types are related to local mixing with connate seawater and are not related to MSR.

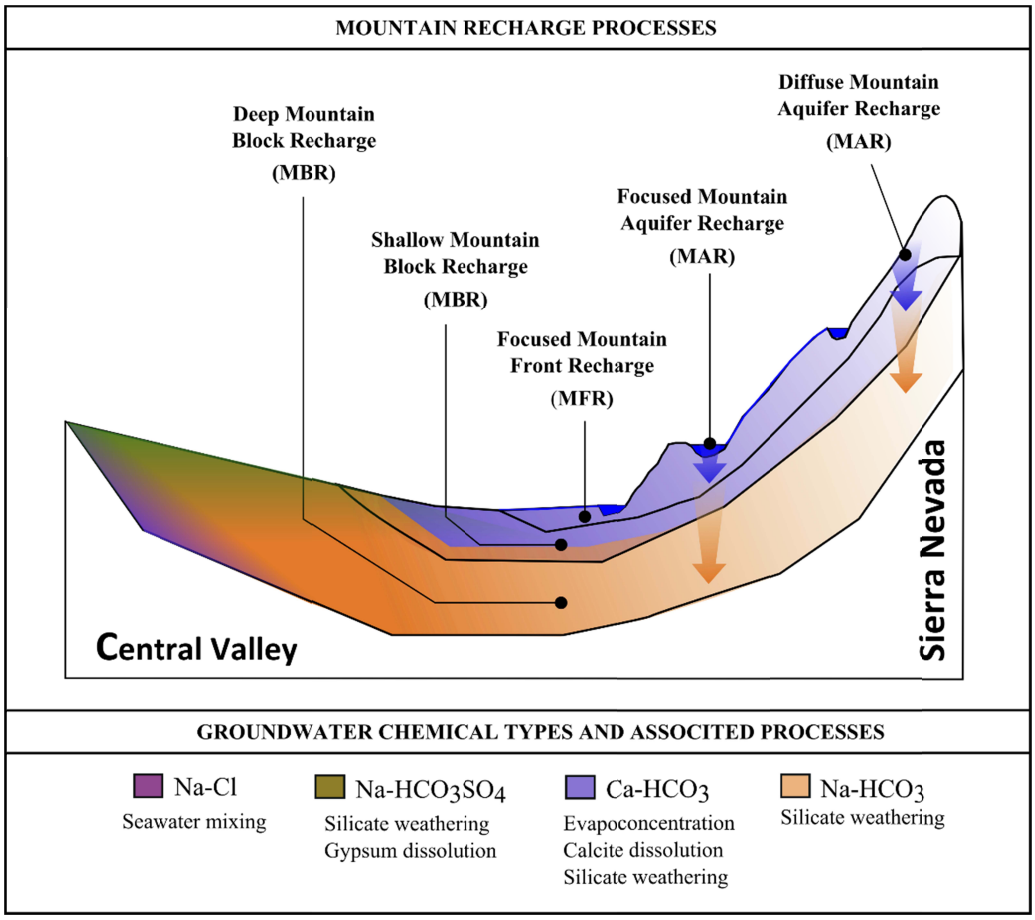

Figure 10. Conceptual illustration of the relation between the five recharge pathways in the study area, along with the main groundwater chemical types and their associated hydrogeochemical processes. Chemical groundwater facies are shown in different colors and polygons represent the spatial distribution of MFR, shallow MBR and deep MBR processes.

3.3. Determining MBR and MFR Contributions via End-member (EMMA) and MIX Analyses

Results of the chemical and isotopic analyses informed end-member selection for the EMMA and groundwater chemistry data are used to determine ratios of MFR and MBR using MIX across the valley aquifer system.

3.3.1. End-member and Solutes Selection for EMMA

To explain the chemical variability of groundwater, different mixing models were developed to find the best end-members and tracers. These models included different combinations of end-members and tracers, and the model selection was based on the percentage of variance explained by the three eigenvectors (EG1, EG2 and EG3) while ensuring that the projected components were enclosed by the end-member triangle at the EG1-EG2 and EG1-EG3 projection space. For the end-member analysis, two general models with 3 and 4 end-members were developed (Table 2). Model 1 consists of an evaporated Ca-HCO_3 groundwater type sample (HLS08) from the

MRA representing MFR, a 0-Tritium Na-HCO_3 sample (KAW07) from the LVA to represent the deep MBR, and a Na-HCO_3SO_4 groundwater type sample (TLA07) from the WVA representing deep MBR with long exposure to water-rock reactions. In addition to end-members in Model 1, Model 2 includes a Ca-Cl groundwater sample (TLA13) from the WVA representing mixing with connate seawater. This sample is not related to the MSR process. All selected end-members are plotted as empty circles in Figure 3b.

In Model 1, the coefficient of determinations between the measured and modeled values of Mg, K, and SO_4 are large ($R^2 \geq 0.75$; RMSE ≤ 0.32). However, poor results are obtained for Cl, Na, alkalinity (RMSE ≥ 1.75), Ca, and pH ($R^2 \leq 0.44$). Model 2 results are satisfactory for Mg, K, and pH ($R^2 \geq 0.77$; RMSE ≤ 0.39) and are significantly better than Model 1 for Ca and Cl ($R^2 \geq 0.72$; RMSE ≤ 0.6). However, further improvement for estimating Na, alkalinity (RMSE ≥ 1.71), and pH ($R^2 \leq 0.2$) is needed. Differences between measured and modeled concentration are related to overestimation of all solutes, except SO_4 (slope, $m<1$, Table 2). Among all parameters in Model 2, pH was the only one with a non-acceptable R^2 (0.1, Table 2). This result suggests that multiple non-linear reactions could affect pH.

To improve Model 2 performance different tracers were added or removed resulting in Model 2a to 2d (Table 2). Removing pH in Model 2a increased the total variance explained by all the solutes by 4% (Table 2). Stable $\delta^{18}O$ (‰), $\delta^{2}H$ (‰), and $\delta^{13}C$ (‰) isotopes were added in Models 2b, 2c, and 2d, respectively. However, very poor R^2 and RMSE are obtained, and the total explained variance decreased to 79%. EMMA analysis seems inappropriate for identifying evaporation using $\delta^{18}O$ (‰) and $\delta^{2}H$ (‰). In addition, poor results for $\delta^{13}C$ (‰) and pH are attributed to multiple, non-linear processes, and local processes affecting the C and H^+ concentrations in groundwater. Finally, Model 2a is selected for the EMMA analysis which only considers the chemical differences among the samples. This means that the evaporated Ca-HCO_3 end-member is representative of MFR and shallow MBR as it is not possible to distinguish non-evaporated Ca-HCO_3.

The composition of three eigenvectors (EG) of Model 2a are plotted in Figure 11 and defined by EG1, EG2 and EG3 in EG1-EG2 and EG2-EG3 spaces shown in Figure 12. Positive EG contributions in Figure 11 are related to changes in samples concentrations plotted on the right side of the 0 value in the EG1-EG2 and EG2-EG3 (Figure 12). Negative contributions are related to changes in samples concentration are on the left side of the 0 value.

Table 2. Results of EMMA analysis: coefficient of determination (R^2), root-mean-squared error (RMSE), slope (m), and total representative variance (%) of major solutes (mol/L), pH and stable $\delta^{18}O$, $\delta^{2}H$, and $\delta^{13}C$ between measured and modeled concentrations for various models. Only subset of models is shown here. *Statistics computed with µmol/L due to low H concentration (<0.001 mol/L) and output format of MIX printing values up to 3 significant digits.

Model	Variables																																	Variance (%)
	Ca			Na			Mg			K			Cl			Alk			SO_4			pH*			$\delta^{18}O$			$\delta^{2}H$			$\delta^{13}C$			
	m	RMSE	R^2	m	RMSE	R^2	m	RMSE	R^2	m	RMSE	R^2	m	RMSE	R^2	m	RMSE	R^2	m	RMSE	R^2	m	RMSE	R^2	m	RMSE	R^2	m	RMSE	R^2	m	RMSE	R^2	
1	0.7	0.7	0.4	0.7	2.4	0.8	0.7	0.2	0.8	0.7	0.03	0.7	0.2	1.8	0.1	0.5	1.9	0.6	0.9	0.3	0.8	0.1	0.1	0.2										82
2	0.7	0.5	0.7	0.7	1.8	0.9	0.7	0.2	0.9	0.8	0.02	0.8	0.9	0.6	0.9	0.6	1.7	0.7	1.2	0.4	0.8	0.1	0.1	0.2										82
2a	0.7	0.5	0.7	0.8	1.9	0.9	0.7	0.2	0.9	0.8	0.00	0.8	1.0	0.6	0.9	0.6	1.7	0.7	1.1	0.4	0.8													86
2b	0.8	0.5	0.7	0.8	1.6	0.9	0.8	0.2	0.9	0.8	0.00	0.8	0.9	0.6	0.9	0.6	1.7	0.7	1.1	0.4	0.8				0.4	1.4	0.4							80
2c	0.7	0.5	0.7	0.8	1.7	0.9	0.7	0.2	0.8	0.8	0.00	0.8	0.9	0.6	0.9	0.6	1.7	0.7	1.1	0.4	0.3							0.4	9.1	0.4				81
2d	0.6	0.6	0.7	0.8	1.7	0.9	0.6	0.3	0.8	0.6	0.00	0.6	0.8	0.6	0.9	0.5	1.8	0.7	1.0	0.3	0.8										0.4	5.5	0.1	79

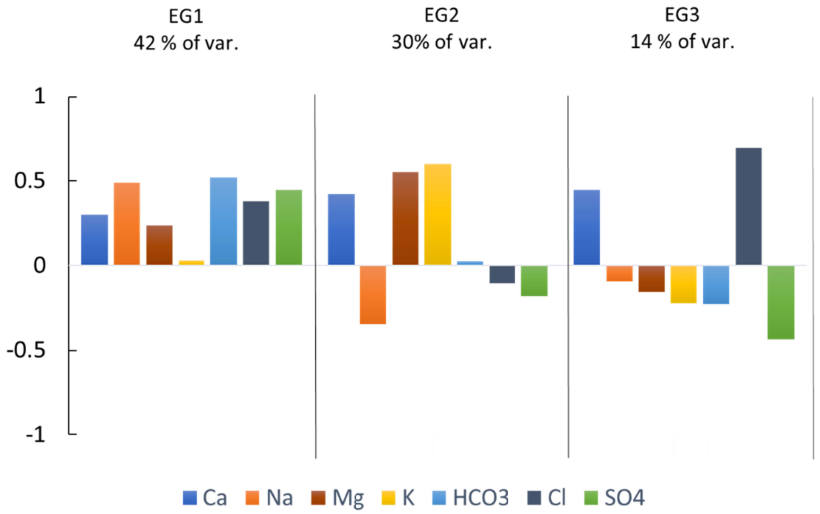

716

717 **Figure 11**. Contribution of eigenvectors 1, 2, and 3 to the total explained variance and relative contribution of each
718 species to each eigenvector.

719 The first eigenvector (EG1) explains 42% of the variance with similar positive contributions
720 from all solutes except K (0.03) (Figure 11). Solutes with a higher positive contribution are Na
721 (0.49), HCO_3 (0.52), SO_4 (0.45) and Cl (0.38). Therefore, EG1 seems to account for the main
722 chemical evolution of groundwater and is associated with evapoconcentration, silicate
723 weathering, calcite, and gypsum dissolution processes. Equal contribution in almost all solutes
724 suggests evapoconcentration is the most representative solute evolution process in EG1 (Figure
725 11).

726 The second eigenvector (EG2) explains 30% of the chemical variability and helps to distinguish
727 among processes responsible for dissolved cation (Ca, Na, Mg, and K) evolution in groundwater.
728 Two major processes identified based on EG2 contributions are biotite weathering (Section
729 3.1.1) responsible for increasing Ca, Mg and K concentrations (positive contribution in EG2,
730 Figure 11), and andesine weathering (Section 3.1.1) for increased dissolved Na (negative
731 contribution in EG2, Figure 11). Although calcite dissolution could also explain higher Ca
732 concentration in EG2, a higher contribution of HCO_3 would be expected.

733 The third eigenvector (EG3) explains 14% of the groundwater chemical variability, and Cl (0.69)
734 and Ca (0.44) are positively contributing to this EG while SO_4 contribution (-0.43) is negative
735 (Figure 11). We attribute the Cl increase to mixing between fresh water and seawater. The
736 positive Ca contribution in EG3 is related to the selection of the Ca-Cl end-member. This end-
737 member is the only sample of this groundwater type and by far has the highest dissolved Cl.
738 Negative SO_4 contribution is attributed to gypsum dissolution even though it is not followed by a
739 negative Ca contribution. We attribute this contradiction to the strong influence of the Ca-Cl
740 end-member. The positioning of non-seawater mixing samples (TLA01 and TLA02) with the
741 highest dissolved SO_4 and Na in Figure 12

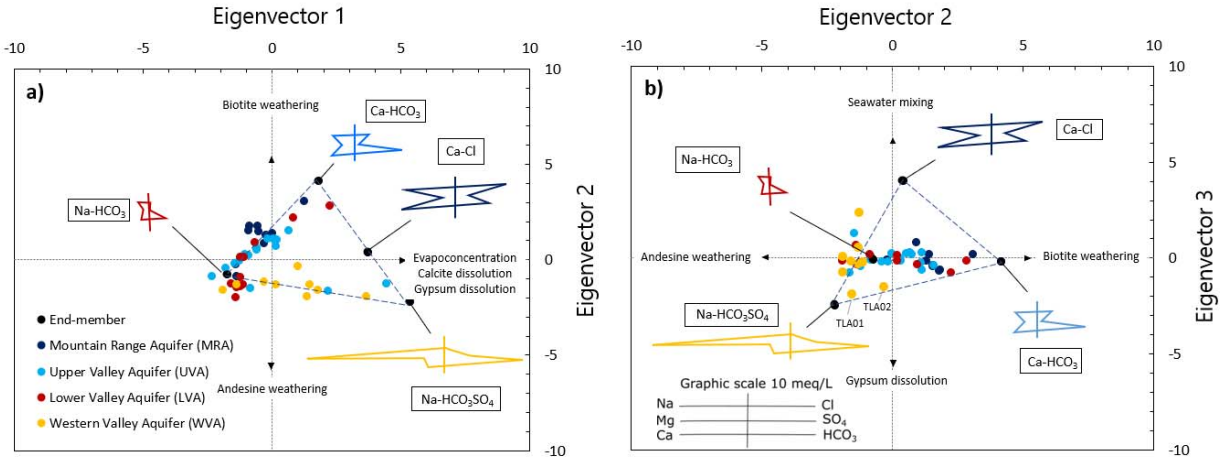

Figure 12a) Projection of solutes concentrations to the first and second eigenvectors space. B) Projection of solutes concentrations to the second and third eigenvectors space. Stiff diagrams represent the ion concentrations of selected end-members.

Based on these results, the main processes that drive Ca-HCO3 groundwater type (representative of MFR and shallow MBR) are biotite weathering, evapoconcentration, calcite dissolution and gypsum dissolution (Figure 12a and Figure 12b). Andesine and biotite weathering are the main processes influencing Na-HCO3 groundwater indicative of MBR (Figure Figure 12a and Figure 12b). The WVA groundwater is represented by the Na-HCO3SO4 groundwater type and is mainly affected by evapoconcentration, calcite dissolution, gypsum dissolution, andesine weathering, and sulfate reduction. Finally, the Ca-Cl groundwater type from this same region represents processes driven by evapoconcentration, calcite dissolution, gypsum dissolution and seawater mixing. These results agree with results obtained in Section 3.1.1 and confirm processes identified for each MSR process.

3.3.2. Improving EMMA by Considering Chemical Reactions

To further improve EMMA, main geochemical processes affecting each eigenvector are identified and chemical reactions are considered in four EMMA models (B, C, D, E and F Table 3). These models aim to reduce the non-conservative behavior of solutes and improve model performance. The model performance is evaluated using RMSE and R^2 instead of the total explained variance. The total explained variance is useful when comparing models with the same number of components. Chemical reactions are represented by conservative **u** components. Components and chemical reactions of each model are reported in Table 3.

765 **Table 3.** Chemical reactions along with the reacting species and conservative components of each model.

	Chemical reactions	Components
A	No chemical reactions	Na, Ca, Mg, K, Cl, SO_4 and alkalinity
B	Andesine dissolution (Eq. 1)	$\boldsymbol{U}_{Andesine} = Ca - 0.7Na$ Mg, K, Cl, SO_4 and alkalinity
C	Andesine dissolution (Eq. 1) Biotite dissolution (Eq. 3)	$\boldsymbol{U}_{Andesine} = Ca - 0.7Na$ $\boldsymbol{U}_{Biotite} = Mg - 3K$ Cl, SO_4 and alkalinity
D	Andesine dissolution (Eq. 1) Gypsum dissolution (Eq. 5)	$\boldsymbol{U}_{And.-Gyp.} = Ca - 0.7Na - SO_4$ Mg, K, Cl and alkalinity
E	Andesine dissolution (Eq. 1) Biotite dissolution (Eq. 3) Gypsum dissolution (Eq. 5)	$\boldsymbol{U}_{And.-Gyp.} = Ca - 0.7Na - SO_4$ $\boldsymbol{U}_{Biotite} = Mg - 3K$ Cl and alkalinity
F	Andesine dissolution (Eq. 1) Biotite dissolution (Eq. 3) Gypsum dissolution (Eq. 5) Calcite dissolution (Eq. 8)	$\boldsymbol{U}_{And.-Gyp.-Calc.} = Ca - 0.7Na - CO_3 - SO_4$ $\boldsymbol{U}_{Biotite} = Mg - 3K$ Cl

766

767 Highly satisfactory results are obtained by incorporating chemical reactions into EMMA instead
768 of chemical solutes as indicated by improved R^2 and RMSE statistics (Table 2, Table 4, and
769 Figure S1). Model F has the best results with R^2= 0.9, 0.1≤RMSE ≤1.3 and slopes between 0.8 to
770 1.1. As the number of components is equal to the number of end-members (three), 100% of the
771 variance is explained by the model. These results further validate all the proposed processes
772 driving the groundwater chemistry in Section 3.1.1. These results agree with Pelizardi et al.
773 (2017) where a synthetic model using simple solutes was compared to a synthetic model using
774 conservative components by computing two objective functions. Their results show that using
775 conservative components instead of simple solutes decreases the objective functions as species
776 affected by chemical reactions usually contribute to a higher percentage of the variance. A recent
777 study by Goyetche et al. (2022) applied the Pelizardi (2017) methodology to a coastal aquifer, by
778 using two conservative u components and one eigenvector. The first u component accounted for
779 four cation exchange and mineral dissolution reactions while the other u component accounted

for eight redox reactions. Their results showed that 97% of the variance could be explained by the model.

Table 5. Results of EMMA analysis: coefficient of determination (R^2), root-mean-squared error (RMSE), and slope (m), of major solutes, pH and stable $\delta^{18}O$, $\delta^{2}H$, and $\delta^{13}C$ between measured and modeled concentrations for models B to F.

Model	Variables																				
	Cl			Alk			SO_4			Mg			K			U-Andesine			U-Biotite		
	R^2	RMSE	m	R^2	RMSE	m	R^2	RMSE	m	R^2	RMSE	m	R^2	RMSE	m	R^2	RMSE	m	R^2	RMSE	m
B	0.8	0.9	0.6	0.6	2.0	0.5	0.7	0.4	0.7	0.8	0.2	0.7	0.5	0.04	0.4	0.8	1.3	0.7			
C	0.6	0.2	0.6	0.6	1.9	0.7	0.6	0.5	1.0							0.6	3.0	0.2	0.6	0.3	0.4
D	0.7	1.5	0.4	0.9	0.7	1.0				0.5	0.3	0.6	0.7	0.03	0.5	0.9	0.9	1.0			
E	0.9	0.7	1.2	0.6	2.0	0.5										0.9	1.1	0.9	0.8	0.2	0.7
F	0.9	0.7	1.1													0.9	1.3	0.8	0.9	0.1	0.9

3.4. Quantifying MBR and MFR Contributions to the Valley Aquifer System

The ratio of each MSR process to total recharge was computed by running MIX for model F (Figure 13). One of the most important results is the high proportion of deep MBR recharging the valley aquifer. Deep MBR represents more than 50% of the UVA and LVA groundwater samples (the Na-HCO3 groundwater type). The high percentage of deep MBR in the UVA wells supports the hypothesis of a mixing zone in the unconfined and confined aquifer contact (Figure 10). The MBR proportion increases up to 70% when the Na-HCO3SO4 groundwater type is also considered. On average, MFR and shallow MBR accounts for 28% of recharge in the UVA, 17% in the LVA, and 20% in the WVA regions. The MFR and shallow MBR contribution decreases with increasing well depth and distance from the mountain front. These results are consistent with the longer flow paths between the WVA wells and the Sierra Nevada. The WVA region has a higher influence of seawater mixing as expected. Higher MBR contribution suggests greater connectivity between the Sierra Nevada and the sedimentary basing groundwater. These results agree with the recent studies highlighting the greater role of MBR compared to MFR (Markovich et al., 2019; Meixner et al., 2016; Aishlin & McNamara, 2011; Manning and Solomon, 2003) and can be used to better constrain future groundwater models for climate change assessment.

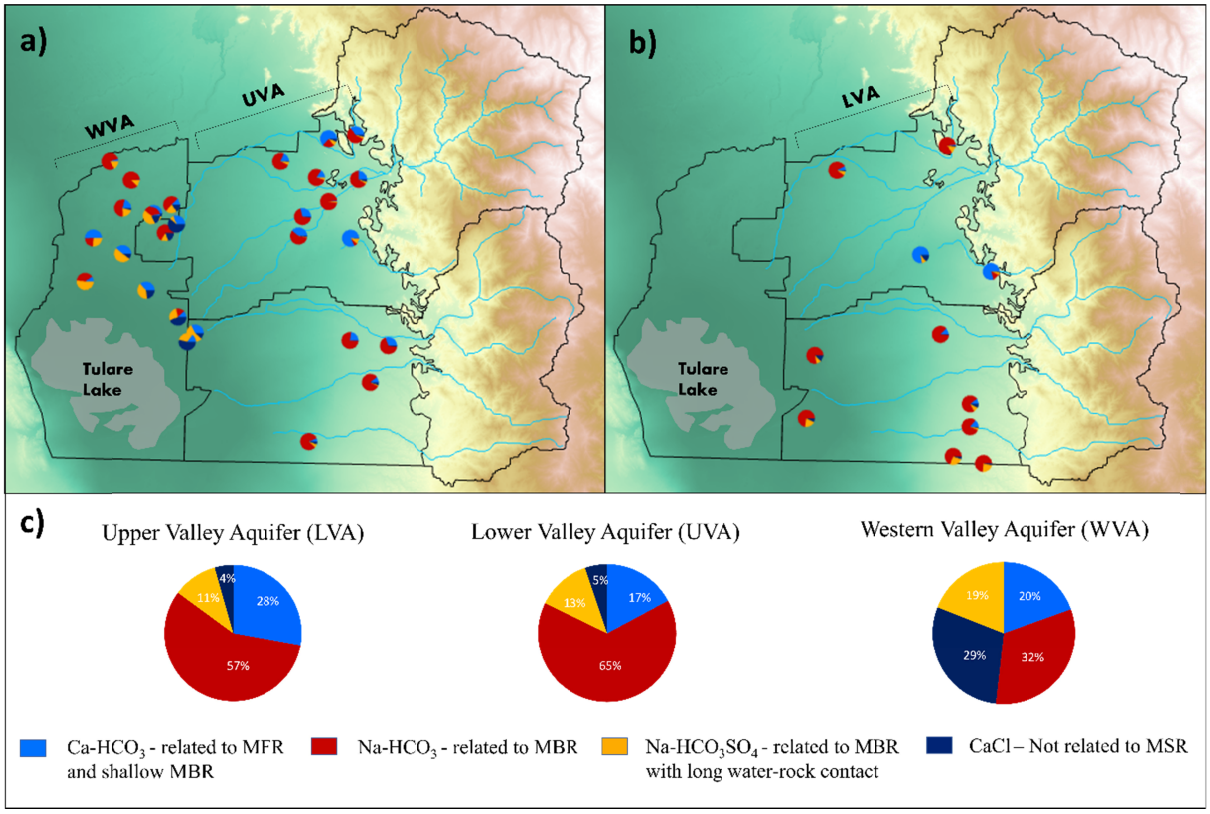

Figure 13. (a) Mixing ratios of each sample in the Upper Valley Aquifer (UVA) and Western Valley Aquifer (WVA) regions (b) and the Lower Valley Aquifer (LVA) region. (c) Average mixing ratios for each groundwater region.

4. Conclusions

We identified major hydrogeochemical processes responsible for the regional groundwater chemistry of the Sierra Nevada and northern Tulare basin to understand MSR pathways. These pathways include diffuse and focused MAR, MFR, and shallow and deep MBR. The main sources of MSR are rain and snowmelt that via direct infiltration through soil or surface water bodies influences mountain-valley groundwater chemistry. Groundwater isogeochemistry data distinguishes three recharge end-members in the valley groundwater that are influenced by hydrologic processes of mountain watersheds. MFR is associated with the evaporated Ca-HCO_3 groundwater type where its composition is influenced by evapoconcentration, edaphic CO_2 dissolution, biotite weathering, and calcite dissolution. Shallow MBR is mainly associated with the non-evaporated Ca-HCO_3 groundwater type and edaphic CO_2 dissolution, biotite weathering, and calcite dissolution affect its chemistry. The main source of shallow MBR is snowmelt infiltration during the peak snowmelt. MFR and shallow MBR recharge the first 100 m of the upper aquifer. Deep MBR is mainly associated with Na-HCO_3 and Na-HCO_3SO_4 groundwater type that are influenced by andesine weathering and gypsum dissolution and recharged during the peak of snowmelt. The MBR recharging the bottom of the confined aquifer is associated with evaporated Na-HCO_3 groundwater type where its chemistry is influenced by andesine weathering and focused MAR from lakes and mountain streams. This groundwater type has a residence time of more than 50 yr, and the influence of focused MAR chemistry highlights the importance of surface water bodies as recharge of deep valley groundwater.

826 EMMA and MIX analysis revealed the spatial distribution of each recharge process associated
827 with the major hydrogeochemical processes in groundwater. Considering four end-members in
828 EMMA produced satisfactory results explaining 86% of the chemical variance. These results
829 were further improved by considering water-rock reactions using conservative chemical
830 components, resulting in significant improvement in model performance. These results highlight
831 the importance of chemical reactions in EMMA and Mix analysis in cases where identifying
832 conservative solutes is challenging. Mixing ratios show that more than 50% of the groundwater
833 system is recharged by MBR originating from the Sierra Nevada. Higher percentage of MBR
834 contribution indicate greater connectivity between the Sierra Nevada and the valley aquifer than
835 previously thought (Meixner et al., 2016). These results have important implications for
836 groundwater resources availability under climate change due to projected changes in the Sierra
837 Nevada snowpack.

838 This study highlights the importance of jointly analyzing groundwater chemistry with isotopes
839 via a multi-tool approach to understand the main factors controlling groundwater systems and
840 identify the main recharge processes. To our knowledge, this is the first comprehensive
841 assessment of mountain block recharge processes in the Sierra Nevada demonstrating the role of
842 mountain aquifers and deep flow paths in recharging Central Valley. Similar studies in other
843 mountain ranges with similar bedrock and geological characteristics will improve understanding
844 of mountain system recharge processes, leading to sustainable groundwater management.

845 **Acknowledgments**

846 This research has been supported by the National Science Foundation CAREER award (No.
847 1944161), and the USDA multistate fund (No. CA-R-ENS-5146-RR). We acknowledge United
848 State Geological Survey (USGS) Groundwater Ambient Monitoring and Assessment (GAMA)
849 program for providing the dataset. We thank Flavia Pelizardi for guidance in constructing the
850 conservative components and for comments on the manuscript.
851
852 All authors declare that they have no conflicts of interest.
853

854 **Open Research**

855 Datasets for this research are available in Table S1 and Table S2 in Supporting Information. The

856 EMMA and MIX code is open source and available on https://h2ogeo.upc.edu/.

857

858

859

860

References

Aishlin, P., & McNamara, J. P. (2011), Bedrock infiltration and mountain block recharge accounting using chloride mass balance. *Hydrological Processes, 25*(12), 1934-1948. doi:10.1002/hyp.7950

Ajami, H., Troch, P. A., Maddock III, T., Meixner, T., & Eastoe, C. (2011). Quantifying mountain block recharge by means of catchment-scale storage-discharge relationships. *Water Resources Research*, *47*(4). doi:10.1029/2010WR009598

Alam, S., Gebremichael, M., Li, R., Dozier, J., & Lettenmaier, D. P. (2019). Climate change impacts on groundwater storage in the Central Valley, California. *Climatic Change*, *157*(3), 387-406. doi:10.1007/s10584-019-02585-5

Appelo, C. A. J., & Postma, D. (2005). *Geochemistry, groundwater and pollution*. CRC press.

Bales, R. C., Molotch, N. P., Painter, T. H., Dettinger, M. D., Rice, R., & Dozier, J. (2006). Mountain hydrology of the western United States. *Water Resources Research*, *42*(8). doi:10.1029/2005WR004387

Barnett, T. P., Adam, J. C., & Lettenmaier, D. P. (2005). Potential impacts of a warming climate on water availability in snow-dominated regions. *Nature*, *438*(7066), 303-309. doi:10.1038/nature04141

Barthold, F. K., Tyralla, C., Schneider, K., Vaché, K. B., Frede, H. G., & Breuer, L. (2011). How many tracers do we need for end member mixing analysis (EMMA)? A sensitivity analysis. *Water Resources Research*, *47*(8). doi:10.1029/2011WR010604

Bazuhair, A. S., & Wood, W. W. (1996). Chloride mass-balance method for estimating ground water recharge in arid areas: examples from western Saudi Arabia. *Journal of Hydrology*, *186*(1-4), 153-159. doi:10.1016/S0022-1694(96)03028-4

Bennett, G.L., V, Fram, M.S., Johnson, T.D., (2017), Groundwater-Quality Data in the Tulare Shallow Aquifer Study Unit, (2014-2015): *Results from the California GAMA Priority Basin Project: US Geological Survey data release*. doi:10.5066/F7BP00W8.

Berghuijs, W. R., Woods, R. A., & Hrachowitz, M. (2014). A precipitation shift from snow towards rain leads to a decrease in streamflow. Nature climate change, 4(7), 583-586. doi:10.1038/nclimate2246

Boiano, D. M., Weeks, D. P., Hemry, T. (2005), Sequoia and Kings Canyon National Parks, California: water resources information and issues overview report. *Technical Report NPS/NRWRD/NRTR 2005/333. National Park Service, Denver, Colorado, USA*.

Christophersen, N., & Hooper, R. P. (1992). Multivariate analysis of stream water chemical data: The use of principal components analysis for the end-member mixing problem. *Water Resources Research*, *28*(1), 99-107. doi:10.1029/91WR02518

Carrera, J., Vázquez-Suñé, E., Castillo, O., & Sánchez-Vila, X. (2004). A methodology to compute mixing ratios with uncertain end-members. *Water resources research*, *40*(12). doi:10.1029/2003WR002263

Clow, D. W., Mast, M. A., Campbell, D. H. (1996), Controls on surface water chemistry in the upper Merced River basin, Yosemite National Park, California. *Hydrological Processes, 10*(5), 727-746. doi:10.1002/(SICI)1099-1085(199605)10:5<727::AID-HYP316>3.0.CO;2-D

Clow D. W., Mast M. A., Bullen T. D., and Turk J. T. (1997) Strontium 87/strontium 86 as a tracer of mineral weathering reactions and calcium sources in an alpine/subalpine watershed, Loch Vale, Colorado. Water Resources Res. 33, 1335–1351.

Coes, A. L., Pool, D. R., Stonestrom, D. A., Constantz, J., Ferre, T., & Leake, S. A. (2007). Ephemeral-stream channel and basin-floor infiltration and recharge in the Sierra Vista subwatershed of the Upper San Pedro Basin, southeastern Arizona. *US Geol Surv Prof Pap*, 253-311.

Craig, H. (1961). Isotopic variations in meteoric waters. *Science*, *133*(3465), 1702-1703. doi: 10.1126/science.133.3465.1702

Davis, G.H., Green, J. H., Olmsted, F. H., & Brown, D. W. (1959). Ground-water conditions and storage capacity in the San Joaquin Valley California (No 1469). *US Government Printing Office.*

De Vries, J. J., & Simmers, I. (2002). Groundwater recharge: an overview of processes and challenges. *Hydrogeology Journal*, *10*(1), 5-17. doi:10.1007/s10040-001-0171-7

Diepenbrock, A. (1933). Mount Poso oil field. *California Oil Fields*, *19*(2), 4-35.

Diffenbaugh, N. S., Swain, D. L., & Touma, D. (2015). Anthropogenic warming has increased drought risk in California. *Proceedings of the National Academy of Sciences*, *112*(13), 3931-3936. doi:10.1073/pnas.1422385112

Elnashar, A., Wang, L., Wu, B., Zhu, W., & Zeng, H. (2020). Synthesis of global actual evapotranspiration from 1982 to 2019. *Earth System Science Data Discussions*, *2020*, 1-42.doi:10.5194/essd-13-447-2021

Faunt, C. C., Sneed, M., Traum, J., & Brandt, J. T. (2016). Water availability and land subsidence in the Central Valley, California, USA. *Hydrogeology Journal*, *24*(3), 675-684. doi:10.1007/s10040-015-1339-x

Feth, J. H. F., Robertson, C. E., Polzer, W. L. (1964), Sources of mineral constituents in water from granitic rocks, Sierra Nevada, California and Nevada. *US Government Printing Office*.

Flint, A. L., Flint, L. E., Hevesi, J. A., & Blainey, J. B. (2004). *Fundamental concepts of recharge in the Desert Southwest: a regional modeling perspective* (Vol. 9, pp. 159-184). Washington, DC: American Geophysical Union.

952 Friedman, I. (1992), Stable isotope composition of waters in southeastern California 1. Modern
953 precipitation. *Journal of Geophysical Research: Atmospheres, 97,* 5795-5812.

954 Frink, J. W., & Kues, H. A. (1954). Corcoran Clay—A Pleistocene lacustrine deposit in San
955 Joaquin Valley, California. *AAPG Bulletin*, *38*(11), 2357-2371.
956
957 Frisbee, M. D., Phillips, F. M., Campbell, A. R., Liu, F., and Sanchez, S. A. (2011), Streamflow
958 generation in a large, alpine watershed in the southern Rocky Mountains of Colorado: Is
959 streamflow generation simply the aggregation of hillslope runoff responses?, Water Resour.
960 Res., 47, W06512, doi:10.1029/2010WR009391.
961
962 Frisbee, M. D., Tolley, D. G., & Wilson, J. L. (2017). Field estimates of groundwater circulation
963 depths in two mountainous watersheds in the western US and the effect of deep circulation on
964 solute concentrations in streamflow. *Water Resources Research*, *53*(4), 2693-2715.
965 doi:10.1002/2016WR019553
966
967 Fujii, R., Swain, W. C. (1995), Areal distribution of selected trace elements, salinity, and major
968 ions in shallow ground water, Tulare Basin, southern San Joaquin Valley, California. *US*
969 *Department of the Interior, US Geological Survey, 95*, 4048.
970
971 Garrels, R.M, & Mackenzie, F.T., (1967), Origin of the chemical composition of springs and
972 lakes, in Equilibrium concepts in natural water systems. *American Chemical Society, Advances*
973 *in Chemistry Series no. 67*, 222-242.doi: 10.1021/ba-1967-0067.ch010
974
975 Gleeson, T., & Manning, A. H. (2008). Regional groundwater flow in mountainous terrain:
976 Three-dimensional simulations of topographic and hydrogeologic controls. *Water Resources*
977 *Research*, *44*(10). doi:10.1029/2008WR006848
978
979 Goodrich, D. C., Williams, D. G., Unkrich, C. L., Hogan, J. F., Scott, R. L., Hultine, K. R., Pool,
980 D., Coes, A., & Miller, S. (2004). Comparison of methods to estimate ephemeral channel
981 recharge, Walnut Gulch, San Pedro River basin, Arizona. *Groundwater recharge in a desert*
982 *environment: the southwestern United States*, *9*, 77-99. doi:10.1029/009WSA06
983
984 Goyetche, T., Luquot, L., Carrera, J., Martínez-Pérez, L., & Folch, A. (2022). Identification and
985 quantification of chemical reactions in a coastal aquifer to assess submarine groundwater
986 discharge composition. *Science of the Total Environment*, *838*, 155978.
987 doi:10.1016/j.scitotenv.2022.155978
988
989 Hem, J. D. (1985). *Study and interpretation of the chemical characteristics of natural*
990 *water* (Vol. 2254). Department of the Interior, US Geological Survey.
991
992 Hilton, G.S., McClelland E.J., Klausing R. L., Kunkel F. (1963), Geology hydrology, and quality
993 of water in the Terra Bella-Lost Hills area, San Joaquin Valley, California. *USGS Open-File*
994 *Report*, 6347, 158.
995

Hooper, R. P. (2003). Diagnostic tools for mixing models of stream water chemistry. *Water Resources Research*, *39*(3). doi:10.1029/2002WR001528

Hooper, R. P., Christophersen, N., & Peters, N. E. (1990). Modelling streamwater chemistry as a mixture of soilwater end-members—An application to the Panola Mountain catchment, Georgia, USA. *Journal of Hydrology*, 116(1-4), 321-343. doi:10.1016/0022-1694(90)90131-G

Hoots, H. W., Bear, T. L., & Kleinpell, W. D. (1954). *Geological summary of the San Joaquin Valley, California*. California, Division of Mines.

Huber, N. K. (1987). *The geologic story of Yosemite National Park* (No. 1595). US Geological Survey.

Huth, A. K., Leydecker, A., Sickman, J. O., Bales, R. C. (2004), A two-component hydrograph separation for three high-elevation catchments in the Sierra Nevada, California. *Hydrological Processes, 18*(9), 1721-1733. doi:10.1002/hyp.1414

Inter-Agency Committee on Land Subsidence in the San Joaquin Valley. (1958). *Progress Report on Land-Subsidence Investigations in the San Joaquin Valley, California, Through 1957*. The Committee.

Kang, S., Knight, R., Goebel, M. (2022), Improved imaging of the large-scale structure of a groundwater system with airborne electromagnetic data. *Water Resources Research, 58*, e2021WR031439. doi:10.1029/2021WR031439

Kendall, C., & Coplen, T. B. (2001). Distribution of oxygen-18 and deuterium in river waters across the United States. Hydrological processes, 15(7), 1363-1393. doi:10.1002/hyp.217

Klausing, R. L., & Lohman, K. E. (1964). Upper Pliocene marine strata on the east side of the San Joaquin Valley, California. *US Geological Survey Professional Paper 475-D*, 14-17.

Lechler, A. R., & Niemi, N. A. (2012), The influence of snow sublimation on the isotopic composition of spring and surface waters in the southwestern United States: Implications for stable isotope–based paleoaltimetry and hydrologic studies. *Bulletin*, *124*(3-4), 318-334.

Liu, Y., & Yamanaka, T. (2012). Tracing groundwater recharge sources in a mountain–plain transitional area using stable isotopes and hydrochemistry. *Journal of Hydrology*, 464, 116-126. doi:0.1016/j.jhydrol.2012.06.053

Lofgren, B. E. & Klausing, R. L. (1969), Land subsidence due to groundwater withdrawal, Tulare-Wasco area, California. *US Government Printing Office*, 437.

Manning, A.H. & Solomon, D.K. (2003). Using noble gases to investigate mountain-front recharge. J. Hydrol. 275, 194–207.

Markovich, K. H., Manning, A. H., Condon, L. E., & McIntosh, J. C. (2019). Mountain-block recharge: A review of current understanding. *Water Resources Research*, *55*(11), 8278-8304. doi:10.1029/2019WR025676

Mast, M. A., Drever, J. I., & Baron, J. (1990). Chemical weathering in the Loch Vale watershed, Rocky Mountain National Park, Colorado. *Water Resources Research*, *26*(12), 2971-2978. doi:10.1029/WR026i012p02971

Maxey, G. B., & Eakin, T. E. (1949). Ground water in White River Valley, White Pine, Nye, and Lincoln Counties, Nevada.

Meade, R. H. (1967). *Petrology of sediments underlying areas of land subsidence in central California* (Vol. 497). US Government Printing Office.

Meixner, T., Manning, A. H., Stonestrom, D. A., Allen, D. M., Ajami, H., Blasch, K. W., Brookfield, A., Castro, C., Clark, J., Gochis, D., Flint, A., Neff, N., Rodell, M., Scanlon, B., Singha, K., & Walvoord, M. A. (2016). Implications of projected climate change for groundwater recharge in the western United States. *Journal of Hydrology*, *534*, 124-138. doi:10.1016/j.jhydrol.2015.12.027

Melack, J. M., Stoddard, J. L., Ochs, C. A. (1985), Major ion chemistry and sensitivity to acid precipitation of Sierra Nevada lakes. *Water Resources Research, 21*(1), 27-32. doi:10.1029/WR021i001p00027

Melack, J. M., Sadro, S., Sickman, J. O., & Dozier, J. (2020). *Lakes and watersheds in the Sierra Nevada of California: Responses to environmental change* (Vol. 5). Univ of California Press.

Molins, S., Carrera, J., Ayora, C., & Saaltink, M. W. (2004). A formulation for decoupling components in reactive transport problems. *Water Resources Research*, *40*(10). doi:10.1029/2003WR002970

Moran, J. E., Esser, B. K., Hillegonds, D., Holtz, M., Roberts, S. K., Singleton, M. J., & Visser, A. (2011). *California GAMA special study: Nitrate fate and transport in the Salinas Valley* (No. LLNL-TR-484186). Lawrence Livermore National Lab. (LLNL), Livermore, CA (United States). doi:10.2172/1122241

NADP. (2022). National Atmospheric Deposition Program, https://nadp.slh.wisc.edu/sites/ntn-ca75/

NOAA. (2022). National Water Model CONUS Retrospective Dataset was accessed on 2022 from https://registry.opendata.aws/nwm-archive.

Park, W. H., and Weddle, J. R. (1959), Correlation study of southern San Joaquin Valley. Summary of operations, *California oil fields, 45*(1), 33-34.

Parkhurst, D. L. (1997). Geochemical mole-balance modeling with uncertain data. *Water Resources Research*, *33*(8), 1957-1970. doi:10.1029/97WR01125

Pelizardi, F., Bea, S. A., Carrera, J., & Vives, L. (2017). Identifying geochemical processes using End Member Mixing Analysis to decouple chemical components for mixing ratio calculations. *Journal of Hydrology*, *550*, 144-156. doi:10.1016/j.jhydrol.2017.04.010

Peng, T. R., Zhan, W. J., Tong, L. T., Chen, C. T., Liu, T. S., & Lu, W. C. (2018). Assessing the recharge process and importance of montane water to adjacent tectonic valley-plain groundwater using a ternary end-member mixing analysis based on isotopic and chemical tracers. *Hydrogeology Journal*, *26*(6), 2041-2055. doi:10.1007/s10040-018-1741-2

Rose, T. P., Davisson, M. L., & Criss, R. E. (1996). Isotope hydrology of voluminous cold springs in fractured rock from an active volcanic region, northeastern California. *Journal of Hydrology*, *179*(1-4), 207-236. doi:10.1016/0022-1694(95)02832-3

Rosenthal, W., & Dozier, J. (1996). Automated mapping of montane snow cover at subpixel resolution from the Landsat Thematic Mapper. *Water Resources Research*, *32*(1), 115-130. doi:10.1029/95WR02718

Rueedi, J., Purtschert, R., Beyerle, U., Alberich, C., & Kipfer, R. (2005). Estimating groundwater mixing ratios and their uncertainties using a statistical multi parameter approach. *Journal of hydrology*, *305*(1-4), 1-14. doi:10.1016/j.jhydrol.2004.06.044

Scanlon, B.R., Reedy, R.C., Stonestrom, D.A., Prudic, D.E., Dennehy, K.F., (2005). Impact of land use and land cover change on groundwater recharge and quality in the southwestern US. Glob. Chang. Biol. 11, 1577–1593. https://doi.org/10.1111/j.1365-2486.2005.01026.x

Scanlon, B. R., Faunt, C. C., Longuevergne, L., Reedy, R. C., Alley, W. M., McGuire, V. L., & McMahon, P. B. (2012). Groundwater depletion and sustainability of irrigation in the US High Plains and Central Valley. *Proceedings of the national academy of sciences*, *109*(24), 9320-9325. doi:10.1073/pnas.1200311109

Schreiner-McGraw, A. P., Ajami, H., & Vivoni, E. R. (2019). Extreme weather events and transmission losses in arid streams. *Environmental Research Letters*, *14*(8), 084002. doi:10.1088/1748-9326/ab2949

Seager, R., Ting, M., Held, I., Kushnir, Y., Lu, J., Vecchi, G., Huang, H., Harnik, N., Leetmaa, A., Lau, N., Li, C., Velez, J., & Naik, N. (2007). Model projections of an imminent transition to a more arid climate in southwestern North America. *Science*, *316*(5828), 1181-1184. doi: 10.1126/science.1139601

Shaw, G. D., Conklin, M. H., Nimz, G. J., Liu, F. (2014), groundwater and surface water flow to the Merced River, Yosemite Valley, California: 36Cl and cl- evidence. *Water Resources Research, 50*(3), 1943–1959. doi:10.1002/2013WR014222

Sisson, T. W., & Moore, J. G. (1984). *Geology of Giant Forest-Lodgepole Area, Sequoia National Park, California*. US Department of the Interior, Geological Survey.

Tobin, B. W., & Schwartz, B. F. (2016). Using periodic hydrologic and geochemical sampling with limited continuous monitoring to characterize remote karst aquifers in the Kaweah River Basin, California, USA. *Hydrological Processes*, *30*(19), 3361-3372. doi:10.1002/hyp.10859

Visser, A., Moran, J. E., Hillegonds, D., Singleton, M. J., Kulongoski, J. T., Belitz, K., & Esser, B. K. (2016). Geostatistical analysis of tritium, groundwater age and other noble gas derived parameters in California. *Water Research*, 91, 314-330. doi:10.1016/j.watres.2016.01.004

Visser, A., Moran, J. E., Singleton, M. J., & Esser, B. K. (2018). Importance of river water recharge to the San Joaquin Valley groundwater system. *Hydrological Processes*, *32*(9), 1202-1213. doi:10.1002/hyp.11468

Viviroli, D., Kummu, M., Meybeck, M., Kallio, M., & Wada, Y. (2020). Increasing dependence of lowland populations on mountain water resources. *Nature Sustainability*, *3*(11), 917-928. doi:10.1038/s41893-020-0559-9

Wahi, A. K., Hogan, J. F., Ekwurzel, B., Baillie, M. N., & Eastoe, C. J. (2008). Geochemical quantification of semiarid mountain recharge. Groundwater, 46(3), 414-425. doi:10.1111/j.1745-6584.2007.00413.x

Wahrhaftig, C., & Birman, J. H. (1965). The Quaternary of the Pacific mountain system in California. In *The Quaternary of the US* (pp. 299-340). Princeton University Press.

Welch, L. A., & Allen, D. M. (2012). Consistency of groundwater flow patterns in mountainous topography: Implications for valley bottom water replenishment and for defining groundwater flow boundaries. *Water Resources Research*, *48*(5). doi:10.1029/2011WR010901

White, A. F., Bullen, T. D., Vivit, D. V., Schulz, M. S., & Clow, D. W. (1999). The role of disseminated calcite in the chemical weathering of granitoid rocks. Geochimica et Cosmochimica Acta, 63(13-14), 1939-1953. doi:10.1016/S0016-7037(99)00082-4

Williams, M., Kattelmann, R., & Melack, J. (1990). Groundwater contributions to the hydrochemistry of an alpine basin. *Hydrology in Mountainous Regions*, *1*, 741-748.

Williams M. W., Brown A. D., and Melack J. M. (1993) Geochemical and hydrologic controls on the composition of surface water in a high-elevation basin, Sierra Nevada, California. Limnol. Oceanogr. 38, 775–797.

Wilson, J. L., & Guan, H. (2004). Mountain-block hydrology and mountain-front recharge. *Groundwater recharge in a desert environment: The Southwestern United States*, *9*, 113-137. doi:10.1029/009WSA08

Xiao, M., Koppa, A., Mekonnen, Z., Pagán, B. R., Zhan, S., Cao, Q., ... & Lettenmaier, D. P. (2017). How much groundwater did California's Central Valley lose during the 2012–2016 drought?. *Geophysical Research Letters*, *44*(10), 4872-4879. doi:10.1002/2017GL073333

1177 Zhu, C., Winterle, J. R., & Love, E. I. (2003). Late Pleistocene and Holocene groundwater
1178 recharge from the chloride mass balance method and chlorine-36 data. *Water Resources*
1179 *Research*, *39*(7). doi:10.1029/2003WR001987